Design and Testing of Experimental Free-Piston Cryogenic Expander

By

Ryan Edward Jones

B.S., Mechanical Engineering
University of South Carolina, 1997

SUBMITTED TO THE DEPARTMENT OF MECHANICAL ENGINEERING
IN PARTIAL FULFILLMENT OF THE REQUIREMENTS FOR THE DEGREE OF
MASTER OF SCIENCE IN MECHANICAL ENGINEERING

AT THE

MASSACHUSETTS INSTITUTE OF TECHNOLOGY

FEBRUARY 1999

© 1999 Massachusetts Institute of Technology
All rights reserved

Signature of Author .....
Department of Mechanical Engineering
January 31, 1999

Certified by .....
Joseph L. Smith, Jr.
Professor of Mechanical Engineering
Thesis Supervisor

Accepted by .....
Ain A. Sonin
Chairman, Department Committee on Graduate Students

ENG
MASSACHUSETTS INSTITUTE OF TECHNOLOGY
JUL 12 1999
LIBRARIES
WITHDRAWN FROM MIT LIBRARIES

Design and Testing of Experimental Free Piston Cryogenic Expander

By

Ryan Edward Jones

Submitted to the Department of Mechanical Engineering
on January 31, 1999 in Partial Fulfillment of the
Requirements for the Degree of Master of Science in
Mechanical Engineering

ABSTRACT

An experimental free piston cryogenic expander was designed and constructed as a part of a feasibility test. Unlike most cryogenic expanders, there were no physical connections for controlling or monitoring the position of the piston. Rather, a linear variable differential transformer (LVDT) was designed and constructed on the outside of the cylinder wall to non-intrusively monitor the piston's position. Signals from the LVDT, pressure transducers and thermocouples were collected by a data acquisition system and integrated into a real-time control routine. The control routine digitally switched valves on the warm and cold ends of the expander to control the pressure-volume relation in the cold end of the expander.

Results from experimental testing were compared with theoretical thermodynamic and dynamic analysis of the single-stage apparatus to determine the expander's performance. Comparisons showed that the expander's behavior closely resembled the theoretical models, and identified design considerations and improvements for a second-generation expander. Although the expander was not insulated for thermal performance, significant cooling was evident under testing conditions.

Thesis Supervisor: Joseph L. Smith, Jr.

Title: Professor of Mechanical Engineering

Acknowledgements

I would like to thank professor Smith for his patience and guidance throughout the project and for giving me that extra kick when I needed it. I would like to thank professor Brisson who saved me on numerous occasions in the lab and loaned me vital equipment in exchange for my first born. I am also grateful to Mike and Bob who were always willing to help me and prevent shrapnel from flying around the shop. To my fellow C.E.L. students, thanks for all the sanity checks and comic relief.

I would like to say thank you to my family, who were forced to listen, and pay the phone bill, to all the good and bad times I have endured. Their love and support have meant more than words can express. To my in-laws, thank you for all the pep talks and confidence you gave me. Most Importantly, I would like to say thank you to my wife, Catherine. Without her love, patience and understanding, I would never have made it. Thank you everyone!

The financial support for this research was provided by both the Starr Fellowship and professor Joseph Smith.

Table of Contents

Nomenclature

ΔE : Change in Internal Energy of a System

ρ : Density of Working Fluid

μ : Viscosity of Working Fluid

A_c : Cross-Sectional Area of Piston

A_o : Area of Orifice in Throttle Valve

A_s : Surface Area of Piston

C_p : Specific Heat Capacity at Constant Pressure

C_v : Specific Heat Capacity at Constant Volume

dP : Differential Pressure

ds : Differential Entropy

dT : Differential Temperature

dV : Differential Volume

FC : Force Acting on Piston in the Cold Region

FS : Force on Piston from Gas Spring in Warm Region

FV : Force Acting of Piston as a Result of Piston Motion

g : Gravitational Acceleration

G : Radial Clearance Between Piston and Cylinder Wall

H : Stroke Length

k : Specific Heat Ratio

m : Mass of Working Fluid

m* : Normalized Mass

m_p : Mass of Piston

P : Pressure

P* : Normalized Pressure

P_A : Intermediate Tank A Pressure

P_B : Intermediate Tank B Pressure

P_{in} : Inlet Line Pressure

P_{out} : Exhaust Line Pressure

Q : Heat Transfer

R : Universal Gas Constant

T : Temperature

t : Time

T_{∞} : Ambient Temperature

T* : Normalized Temperature

T_{in} : Inlet Line Temperature

T_{out} : Exhaust Line Temperature

v : Voltage

V : Volume

V* : Normalized Volume

V_{max} : Maximum Volume of Cylinder

V_{tank} : Volume of Intermediate Pressure Tank

W : Work Transfer

List of Figures and Tables

1 Introduction

1.1 Background

Cryogenic engineering utilizes low-temperature refrigeration processes for numerous research and practical applications. These areas range from studying material properties at extreme temperatures to commercial manufacturing and bottling of gases. As in any industry, the need for these processes fuels the research into developing equipment and methods of obtaining cryogenic temperatures more efficiently and reliably. With improved designs and lower cost, cryogenic refrigerators will become an integral and necessary part of our technological society.

There are three common process used to obtain cryogenic temperatures: evaporation, isenthalpic expansion and isentropic expansion. Depending on the application and requirements of the system, cryogenic systems may incorporate any combination of these processes. This research project focused on the design and construction of a free-piston expander to isentropically cool the working fluid.

1.1.1 Expansion Engines

The first law of thermodynamics states that the change in internal energy of a system equals the net flow of energy across the system boundary. For a steady-state closed system, the first law of thermodynamics may be written in the form,

$$\Delta E = Q - W$$

Eqt 1

where Q represents heat transfer into the system and W represents work done by the system. One can see that if work is removed from a system adiabatically, the internal energy of the system must decrease. However, in an isentropic expansion, both the pressure and volume are changed simultaneously. To see the effect of an isentropic process, the second law of thermodynamics must be employed.

The second law of thermodynamics deals with the entropy of a system. Unlike energy, which is conserved, entropy may be generated in an isolated system. Depending on the rate of the processes and methods of heat transfer within a system, the change in entropy over time for an isolated system must be greater than or equal to zero. Although all processes realistically generate entropy, through careful design, the entropy generation can be

minimized such that the process can be modeled as reversible. For an adiabatic, reversible process involving an ideal gas, the second law of thermodynamics

$$\frac{T_2}{T_1} = \left(\frac{P_2}{P_1}\right)^{\frac{k-1}{k}}$$

Eqt 2

illustrates that the temperature ratio between states one and two is a function of the pressure ratio at those states. Since equation 2 is written for an ideal gas, k represents the specific heat ratio, C_p/C_v. This isentropic decrease in temperature was the basis for both the design and analysis of the free-piston expander.

The most general setup for an expansion engine involves a piston that is driven by an external motor. This general process begins by charging a region under a piston. The piston, which is attached to an external driving mechanism, expands the gas isentropically. Once the pressure in the expansion region reaches the exhaust line pressure, the exhaust valve opens and the piston sweeps the cooled gas out of the expander. The work transferred from the expanding gas is rejected to the driving mechanism through the piston. Although all expansion engines need some method of transferring energy in the form of work away from the cold region, it is not always necessary to have physical linkages to an external driver.

This project dealt with a free-piston design for an expansion engine, which involved expanding the gas similar to the method described above, but without a piston connected directly to an external driver. This free-piston design used a pressure differential across the piston to control its motion and extract work from the working fluid. Advantages of the free piston expander over contemporary expanders included fewer moving part, greater dependability and a system that could be sealed to prevent loss of the working fluid over time.

1.2 Project Objective

The objective of this project was to design and construct an experimental free-piston cryogenic expander. Since the free-piston expander was controlled and timed without physical connections, two particular aspects of the system's behavior needed to be investigated. First, could a free-piston expander be constructed and dynamically controlled reliably? Second, how closely would the thermodynamic behavior of the expander reflect the theoretical models developed for a single stage apparatus?

1.3 Expander Cycle

To begin a discussion on the expander, an overall description of the cycle is required. Shown in Figure 1, the system schematic illustrated a piston and cylinder arrangement attached to two intermediate pressure tanks, modeled as constant pressure reservoirs. For the purpose of discussion, tank A was at a higher pressure than tank B. These tanks were never in direct communication with each other. The working fluid, N_2 gas, could only flow between the tanks via the warm region of the expander. The Nitrogen, which passed into to or out of the warm region, passed through both a throttle valve and a 5-port, 2-way spool valve used to select the intermediate pressure tank that was connected to the warm end. 2-way valves were located on the inlet and exhaust ports in the cold region of the expander to control the gas flow.

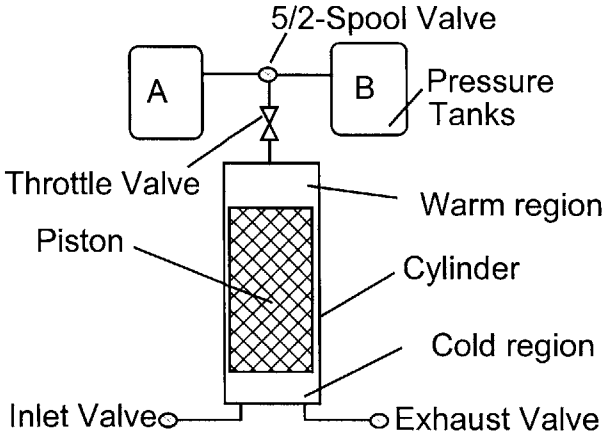

Figure 1: Schematic of Free-Piston Expander

In the actual system, the throttles and 5/2-spool valve were integrated into a warm end assembly that sealed the top of the cylinder. A complete discussion of the details of the system design will be reserved for chapter 3.

To understand the operation of the expander, consider the pressure verses volume plot illustrated in Figure 2. This P-V diagram represented the idealized cycle for the cold region of the expander. Just prior to state 8, the piston in Figure 1was resting on the bottom of the cylinder, and there was no working fluid in the cold region. Both the inlet and exhaust valves were closed, and the warm region was connected to tank A. When the pressure in the cylinder equaled the pressure in tank A, the inlet valve was opened and the pressure jumped to the inlet line pressure before there was any motion of the piston. This was the labeled state 1 in Figure 2. There was now a pressure differential across the piston, which induced motion. The piston moved upward rapidly until the pressure in the

warm region reached P_{in} and equilibrium was established. For the purpose of this explanation, the piston was assumed to have no mass and consequently, vibration was neglected.

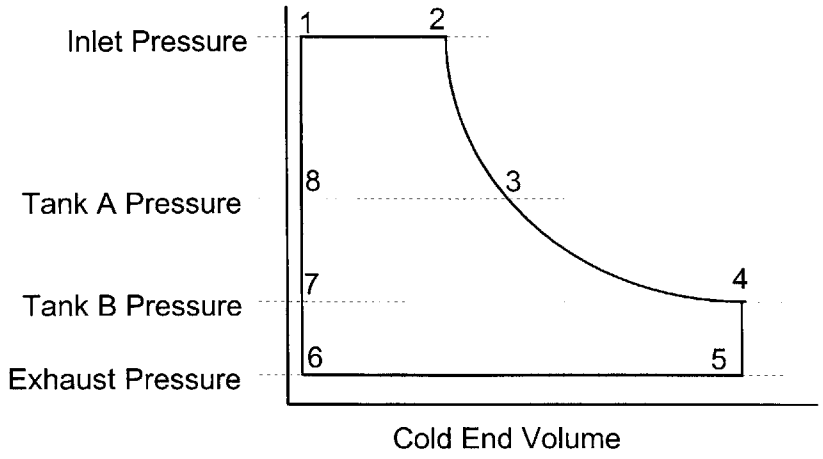

Figure 2: Ideal P-V Relation for Cold Region of Expander

There was now a pressure drop across the throttle valve since $P_{warm} = P_{in}$ and $P_A < P_{in}$. As the compressed gas in the warm region was throttled into tank A, more high-pressure gas entered the cold region to maintain pressure equilibrium. This charging process continued until the volume in the cold region reached that of a preset value, denoted by V_2. This preset value at state 2 was the only adjustable parameter in the actual system for a given inlet and exhaust pressure. Once the system reached state 2, the inlet valve was closed and the isentropic expansion began.

Immediately after the inlet valve was closed, the pressure in both the cold and warm region equaled the inlet line pressure. As the compressed gas in the warm region continued to be throttled into tank A, the pressure in the cylinder dropped. When the cylinder pressure equaled that of tank A, state 3, the 5/2-spool valve was toggled to allow more decompression into tank B. This continued expansion between states 3 and 4 was also isentropic, which resulted in an additional temperature drop. At state 4, it was assumed that the cylinder pressure reached that of tank B as the piston reached top dead center simultaneously. At this point, the exit valve was opened. The blow down process, state 4 to 5, was not accompanied by any motion of the piston because there was zero void space in the warm region at top dead center and there was no gas to expand. The piston began to sweep out the expanded gas in the cold region as gas from tank B flowed through the throttle valve to recharge the warm region. When the piston reached the bottom of the stroke, state 6, the exit valve was closed, allowing the pressure in the cylinder to increase

to that of tank B. At state 7, the 5/2-spool valve toggled back to tank A and gas continued to charge the cylinder through the throttle valve until the pressure in the cylinder equaled P_A, at which time the cycle repeated.

1.4 Project Phases

To investigate the free-piston expander, the project was divided into four stages of development. The first stage was to develop models and optimization routines to analyze the performance of the expander. Next, the expander apparatus was designed and fabricated using an on-sight machine shop. With the apparatus physically constructed, the emphasis shifted to instrumentation and development of a control routine to automate the cycle. Finally, data was collected for analysis and compared with the optimized models.

1.4.1 Modeling and Optimization

To investigate the performance of the free-piston expander, thermodynamic analysis of the cycle was used to predict the temperature drop of the working fluid under various operating conditions. Concurrently with the modeling, optimization routines were developed to determine the optimum design parameters of the expander. Through these optimization routines, the stability and steady-state cyclic operating conditions of the system were also investigated.

1.4.2 Fabrication and Assembly

With the theoretical modeling complete, the design and fabrication process began. Many components of the expander, including the cylinder and cold-end actuators were from previous experiments. A critical component of the free piston design was the warm end assembly, which controlled the switching for the intermediate pressure expansions and dissipated the work as heat by throttling the compressed nitrogen in the warm-end of the cylinder. The piston and non-intrusive position sensing equipment were also integrated into the system. All components for the project were machined in an on-sight machine shop and assembled on an existing test stand.

1.4.3 Instrumentation and Control

A major concern of the free-piston expander, was the reliable control and data acquisition during the cycle. To provide real-time control and feedback of the system's operation, data was continuously sampled and checked to determine appropriate switches for the system. Essential to the control of the system was the position of the piston

inside the cylinder. To acquire this information, a linear variable differential transformer (LVDT) was designed and integrated into the apparatus.

In addition to controlling the expander, data needed to be collected on the thermodynamic behavior of the system to compare with the theoretical models generated in stage 1 of the project. The control program collected data over several cycles and downloaded the information to floppy disks for manipulation.

1.4.4 Testing and Analysis

The final stage of the project consisted of testing the expander under various operating conditions. The different test setups were intended to provide information about the actual performance of the system and it's limitations, which identified design considerations for the second-generation expander. The raw data obtained from the experiments was imported into a data manipulation worksheet, which provided useful graphical results illustrating the cycle's processes.

1.4.5 Results

All analytical design results and experimental results are presented and discussed in chapter 4.

2 Expander Modeling and Optimization

The first stage of the project was to create a thermodynamic model of the expander cycle and optimize the system's parameters for maximum cooling. Before the cycle model was developed, the property relations of an isentropic process were developed for an ideal gas. The next step involved developing the governing equations for the cycle processes and non-dimensionalizing the equations to provide a more general analysis. The equations were then entered into a worksheet and various system configurations were optimized. Finally, a dynamic model of the piston during the blow-in process was developed to investigate the system's dynamic response and vibration during rapid processes in the cycle.

2.1 Isentropic processes

It was established that adiabatic expansions of a system remove energy from the system. It was also shown that the second law provided a quantitative analysis of this cooling effect. This section was devoted to developing the isentropic relations upon which the thermodynamic model was developed.

To begin, entropy was defined as a function of temperature, T, and volume, V. Taking partial derivatives of the respective variables resulted in equation 3.

$$ds = \left(\frac{\delta s}{\delta T}\right) dT + \left(\frac{\delta s}{\delta V}\right) \cdot dV$$

Eqt 3

Substituting the appropriate Maxwell relations and the constitutive relation for an ideal gas into equation 3, the differential pressure-volume relation for an ideal gas became equation 4.

$$C_v \cdot \frac{dP}{P} + C_p \cdot \frac{dV}{V} = 0$$

Eqt 4

Integrating equation 4 and rearranging the variables, a relationship between the volume and pressure ratios during an isentropic process for a ideal gas resulted as shown in equation 5 for constant values of C_p and C_v.

$$\frac{P_2}{P_1} = \left(\frac{V_1}{V_2}\right)^k$$

Eqt 5

Substituting equation 5 into the work integral

$$W_{out} = \int_{\bullet}^{\bullet} P\,dV$$

Eqt 6

and evaluating it from any state 1 to 2 resulted in the following.

$$W_{out} = \frac{P_1 \cdot V_1}{k-1} \cdot \left[1 - \left(\frac{V_1}{V_2}\right)^{k-1}\right]$$

Eqt 7

Equation 7 represented the maximum work attainable from an isentropic expansion. Although all of the energy was unattainable due to friction losses and irreversibilities, equation 7 provided a means by which to judge the expander's performance.

2.2 Thermodynamic modeling

2.2.1 Rubber Geometry

In order to evaluate the cooling effect of the free-piston expansion cycle, a thermodynamic model of the system was developed. An evaluation of the cycle, which related both the warm and cold regions, resulted in a set of equations for the pressure, volume, mass and temperature of the system at each state. The First model that was developed involved "rubber geometry". This meant that during the final isentropic expansion, the piston always reached top dead center at the same instance that the pressure in the warm region equalized with the pressure tank B.

The rubber geometry model began by analyzing the process from state 8 to 1, the blow-in process. Unlike the ideal process in Figure 2, the model included a volume change associated with the sudden change in pressure.

Because this process occured very rapidly, the warm region of the expander was modeled as a closed system, which went through an isentropic compression. However, the cold region, which had zero volume at state 8, was modeled as an open system that expanded. The governing equations for both the warm and cold regions were as follows for the blow-in process.

Cold region:

$$m_1 \cdot C_v \cdot T_1 = -W_{outc} + C_p \cdot T_{in} \cdot m_1$$

Eqt 8

Warm region:

$$m_1 \cdot C_v \cdot (T_1 - T_8) = -\int_8^1 P\,dV = -W_{outw}$$

Eqt 9

$$\frac{T_1}{T_8} = \left(\frac{P_1}{P_8}\right)^{\frac{k-1}{k}}$$

Eqt 10

These equations combined with the ideal gas law and the fact that $W_{outc}=-W_{outw}$, yielded the equilibrium equations for state 1.

The next process, from state 1 to 2, was the charging process. During this time, the cold region was modeled as an open system with constant pressure expansion. At state 2, the pressure was still equal to the inlet line pressure and the volume of the cold region was a preset parameter, denoted by the V_2. A first law analysis of the cold region, equation 11, only contained two unknowns, the temperature and mass at state 2.

$$m_2 \cdot C_v \cdot T_2 - m_1 \cdot C_v \cdot T_1 = -P_{in}(V_2 - V_1) + C_p \cdot T_{in} \cdot (m_2 - m_1)$$

Eqt 11

Using the ideal gas law to relate the mass and temperature of the working fluid at state 2, the equation could be rearranged to solve for the equilibrium properties at state 2.

To solve for state 2 in the warm region, consider the system illustrated in Figure 3.

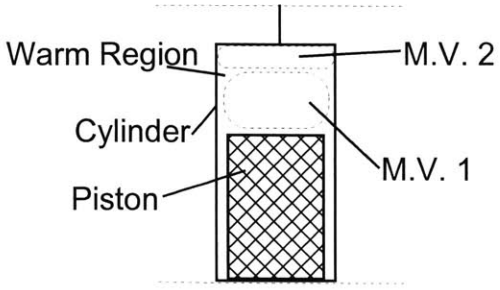

Figure 3: Warm Region Model from State 1→2

The portion of gas contained in material volume 2 was throttled into tank A, and material volume 1 defined the gas that remained in the warm region of the cylinder. A second law analysis of material volume 1 revealed that the warm region temperature remained constant from state 1 to 2. Using this result and the ideal gas relation, it was shown that the mass ratio from state 1 to 2 equaled the volume ratio.

Recall that the inlet valve was closed at state 2, and the first isentropic expansion began. For this process, the cold region was modeled as a closed system that was governed by the following equations.

$$ds = 0 = C_p \cdot \ln\left(\frac{T_3}{T_2}\right) - R \cdot \ln\left(\frac{P_3}{P_2}\right)$$

Eqt 12

$$ds = 0 = C_p \cdot \ln\left(\frac{V_3}{V_2}\right) + C_v \cdot \ln\left(\frac{P_3}{P_2}\right)$$

Eqt 13

In both equation 12 and 13, there was one unknown, which was solved for directly to determine all the properties in the cold region at state 3. To model the warm region during the process from state 2 to 3, a similar material volume approach as shown in Figure 3, was employed. In this situation, the same isentropic relations used for the cold region, were applied to the region labeled material volume 1 in Figure 3. All of the isentropic expansions throughout the cycle were modeled in this same manner. Although the free-piston system was constructed to allow for two isentropic expansions, models, which were discussed in section 4.1.1, were developed for multiple tanks.

During the final isentropic expansion, the rubber geometry model assumed that the warm region volume decreased to zero simultaneously with the pressure differential across the throttle valve. Consequently, there was zero volume in the warm region and no movement from the piston when the pressure in the cold region suddenly dropped as the exhaust valve opened. However, there was a temperature drop associated with this sudden pressure drop in the cold region. To analyze the blow-down and discharge processes, consider the diagram shown in Figure 4.

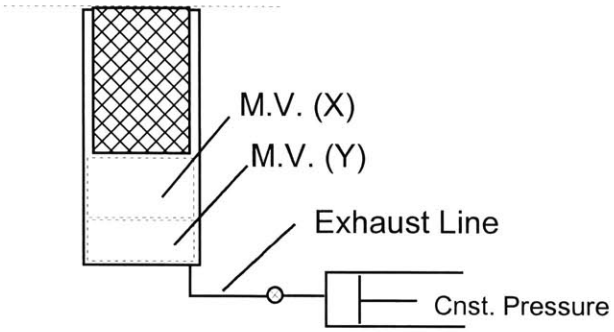

Figure 4: Cold Region Model from state 4→5 and 5→6

Similar to the warm-end material volume analysis during the isentropic expansions, the cold region was divided into two material volumes, shown in Figure 4. This illustration represented the system at state 4, where the sum of the volumes occupied by X and Y together equaled the maximum volume of the cylinder. Material volume X represented the mass that remained in the cylinder immediately after the blow-down process from state 4 to 5. Material volume Y was the mass that was removed from the cold region during this process. For modeling purposes, there was an isentropic expansion of material volume X and a constant pressure expansion of material volume Y as it entered the exhaust line. The resulting first law analysis of the combined subsystems is shown in equation 14.

$$\left[\left(m_{x5}\cdot T_{x5} + m_{y5}\cdot T_{y5}\right) - m_4\cdot T_4\right]\cdot C_v = -P_{out}\cdot V_{y5}$$

Eqt 14

Isentropic expansion relations were used to obtain all properties of material volume X at state 5. The ideal gas law was used to change the constant pressure work term to a mass and temperature relation for material volume Y. Finally, the mass of subsystem Y was eliminated by relating it to the mass at state 4 and subsystem X, which had been completely determined. The only unknown left was the temperature of control mass Y at state 5, which could

be solved for explicitly from equation 14. The cooling effect of the blow-down process was the first time the mass in the cold region became a factor. In all of the other processes, the temperature ratios were independent of the mass in the cold region of the expander.

The next process involved the discharge of the cooled gas and charging of the warm region with gas throttled in from the low-pressure intermediate tank. The cold region process was modeled as an open system, and a first law analysis showed that the work input to the system from the falling piston was used to exhaust the cooled gas. Consequently, there was no temperature change in the cold region from state 5 to 6. However, the two subsystems shown in Figure 4 were mixed in the exhaust line at state 6. A first law analysis of this process, equation 15, showed that the resulting final temperature, of the

$$\left(m_x + m_y\right) T_6 = \left(m_{x5} \cdot T_{x5} + m_{y5} \cdot T_{y5}\right)$$

Eqt 15

working fluid at state 6, was a mass weighted average of the two temperatures found in state 5.

To solve for the warm region properties at state 6, the set of subsystems shown in Figure 5 was analyzed. Subsystems labeled B and C were modeled as material volumes, while subsystem E was modeled as an open system. As before, all systems were assumed adiabatic, permitting only work and mass transfer. A

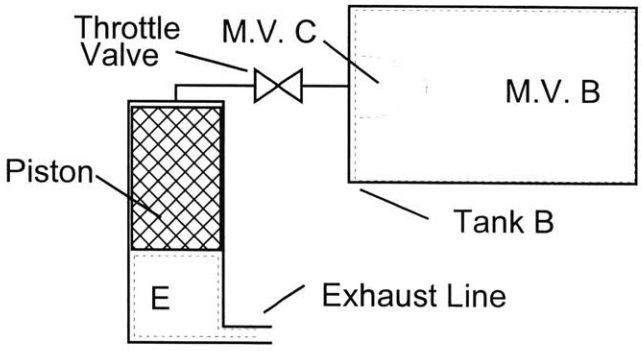

Figure 5: Subsystems for discharge process 5→6

first law analysis of Figure 5 revealed that there was no temperature change in material volume C as it was throttled into the warm region. This was a result of zero void space in the warm region at state 5 and the modeling assumption that all the fluid in the intermediate pressure tank was equaled to the ambient temperature. Once the expander system reached state 6, the exhaust valve was closed, and the piston remained at rest on the bottom of the cylinder from state 6 through state 8.

During this time, the working fluid in the intermediate tanks was used to pressurize the warm region of the expander. From state 6 to 7, gas from the low-pressure tank flowed through the throttle valve and into the warm region. Figure 6 illustrated how this process was modeled.

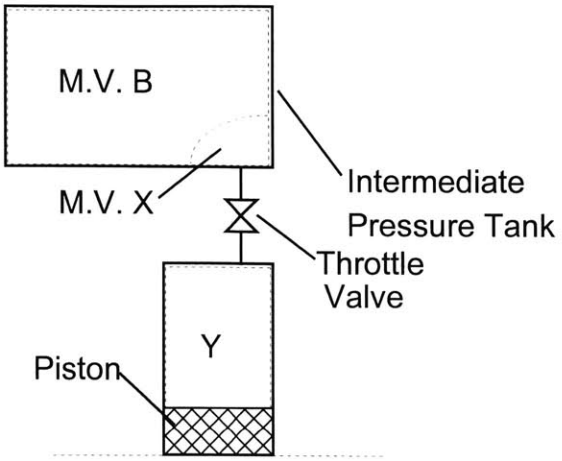

Figure 6: Warm Region Charging Process 6→7 and 7→8

Subsystem B was a constant pressure material volume that compressed the mass of subsystem X into control volume Y.

Again, a first law analysis combined with the ideal gas law and conservation of mass resulted in an explicit equation for the temperature of the warm region at state 7. At this time in the cycle, the pressure in the cylinder equaled that of the low-pressure intermediate tank and the volume of the warm region equaled V_{max}. By toggling the 5/2-spool valve, the next intermediate tank began to charge the pressure in the cylinder.

The process from state 7 to 8 was analyzed in the same manner. Recall that this system only consisted of two intermediate pressure tanks, but this analysis could easily be adapted to multiple intermediate pressure tanks.

Once the cylinder was completely charged to P_A, the cycle began again. The state equations obtained from this analysis were then used to program the optimization routines, which are discussed later.

2.2.2 Fixed Geometry

The rubber geometry analysis assumed that the system processes matched at state 4. This meant that the piston reached top dead center simultaneously with the cylinder pressure equalizing with the low-pressure intermediate tank. In reality, the size of the cylinder was fixed, and depending on the relation between V_2 and P_B, the piston would either reach the top of the stroke too soon, high stroke, or never reach the top at all, low stroke. To

understand the behavior of the free-piston expander, fixed geometry models were developed in a similar manner to the rubber geometry model.

The first case considered was when the piston reached top dead center prior to the pressure in the warm region dropping to that of the low-pressure intermediate tank. Figure 7 depicted the pressure-volume relation

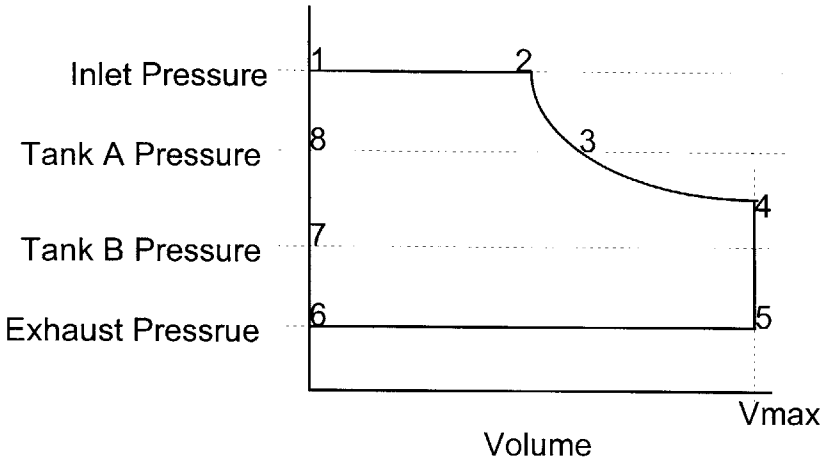

Figure 7: Ideal P-V Relation for High Stroke

for the cold region of the expander when the piston's stroke was too high. In this instance, state 4 and state5 had to be reevaluated to determine the behavior of the system. As the system approached state 4, rather than both the pressure and volume being known, only the volume of the system was known. To evaluate the properties of the system , equation 2 and equation 5 were equated to yield equation 16.

$$\frac{T_4}{T_3} = \left(\frac{V_3}{V_4}\right)^{k-1}$$

Eqt 16

With equations 5 and 16, all the properties of the cold region at state 4 were determined as a function of known volume ratios. Since the warm region volume, as stated, equaled zero, the process from state 4 to 5 in the high stroke model, was modeled the same as the rubber geometry system. All other processes in the high stroke model were treated the same as in the rubber geometry model.

The last scenario considered was a situation in which the relation between V_2 and P_b, resulted in a low stroke for the piston. Figure 8 illustrated the pressure-volume relation for the expander cycle in the cold region.

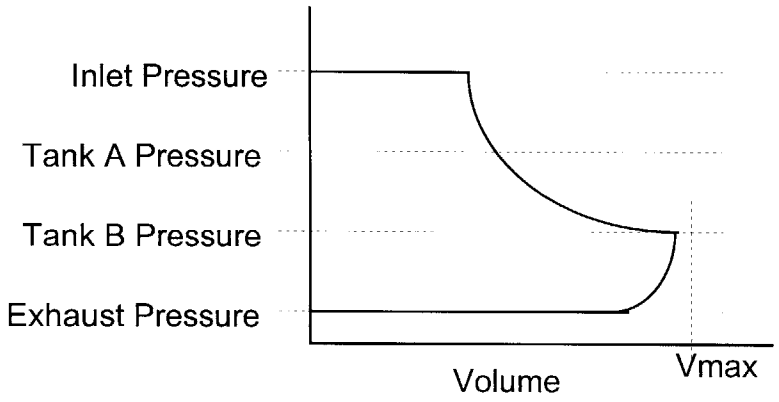

Figure 8: Ideal P-V Relation for Low Stroke

In this situation, the pressure in the cold region decreased to P_B before the piston reached top dead center. The isentropic expansion from state 3 to 4 was modeled the same as in the rubber geometry scenario. However, at state 4, there was still a finite volume in the warm region. Therefore, when the exhaust valve was opened, the piston suddenly dropped, expanding the gas remaining in the warm region until the pressure equaled that of the exhaust line. During the process from state 4 to 5, the warm region was modeled isentropicaly, and the cold region was modeled like the rubber geometry model, accounting for the work transfer from the moving piston.

2.3 Optimization

With all the state equations know for the free-piston expander cycle, it was necessary to analyze the system's behavior under various conditions. These equations were first normalized to various system parameters to provide a generalized analysis. The equations were then solved with the Microsoft Excel solver, which allowed target values, adjustable system parameters, and system constraints to be entered. The resulting steady-state cyclic operating conditions were then tested for stability to determine if non-equilibrium conditions would return to a stable equilibrium.

Before optimizing the state equations, they were normalized to certain system parameters. All temperature variables were normalized to T_{in}, the temperature of the gas entering the cold region of the expander. All pressures were normalized to the inlet line pressure, P_{in}. The volume variables were normalized to V_{max}, the maximum volume of the cylinder occupied by the working fluid. Finally, all the mass variables were normalized to M_{ref}, defined by the ideal gas relation in equation 17.

$$M_{ref} = \frac{P_{in} \cdot V_{max}}{R \cdot T_{in}}$$

Eqt 17

The normalized equations for all three models were entered into a spreadsheet for manipulation. Appendix A contains all of the normalized state equations for the free-piston expander.

The objective of the optimization routine was to minimize the value of $T^*_{out}=f(V^*_2, P^*_A, P^*_B)$ by varying the three independent variables. These independent variables were the volume of the cold region at state 2 and the pressures in the intermediate pressure tanks. These adjustable parameters were subject to the equilibrium constraint that the net mass flow into the intermediate pressure tanks over one cycle must equal zero. The fixed system parameters in the optimization routine were the exhaust line to inlet line pressure ratio and the ambient to inlet line temperature ratio, P^*_{out} and T^*_{∞}.

The rubber geometry model was considered first. For the rubber geometry model, the non-linear equilibrium constraint was only a function of the pressures in the two intermediate tanks. This fact, coupled with the constraint that the stroke must be matched, allowed the final temperature of the working fluid, T^*_{out}, to be optimized as a function of only one variable. Therefore, in addition to the spreadsheet solution, a single algebraic expression for T^*_{out} of the rubber geometry model was developed and optimized. The worksheet for this single expression is shown in detail in Appendix B.

In addition, models for systems with three and four intermediate pressure tanks were also developed for the rubber geometry model. These models were used to determine if the improved temperature drop of the working fluid for multiple tanks was significant enough to warrant experimental testing.

The fixed geometry models were considered next. These two models, described earlier, did not provide an optimization routine as a function of only one variable. The value of T^*_{out} for the fixed geometry models was

effected by all three independent parameters, and was best optimized by iteration of these parameters in the spreadsheets. There were numerous combinations of the independent variables that satisfied the equilibrium constraint. As expected, only one of the combinations provided optimum cooling for the working fluid.

In addition to the steady state cyclic conditions of the system, the stability of these states were also investigated. To conduct the stability test, non-equilibrium conditions for the system were entered into the spreadsheet. Using the results of the program, corresponding small iterations in the independent system parameters were made to observe if the system returned to an equilibrium condition or if the system became unstable and failed to recover. Coupled with the stability analysis, were the relative sizes of the intermediate pressure tanks and their effect on the recovery of the system from non-equilibrium cyclic operation. Optimization results are discussed in section 4.1

2.4 Dynamic Modeling

When the free-piston expander was designed, it was critical to understand the piston's behavior during the cycle. Since there was no connection to an external driver, control of the piston was dependent on other system processes and rates. Most of the processes in the expander cycle were assumed quasi-static, except for the blow-in and blow-down process. During these processes there were sudden changes in the pressure differential across the piston, and it was necessary to determine the dynamics of the system to develop an effective control routine.

To model the blow-in process, consider the free body diagram shown below, Figure 9. In this diagram,

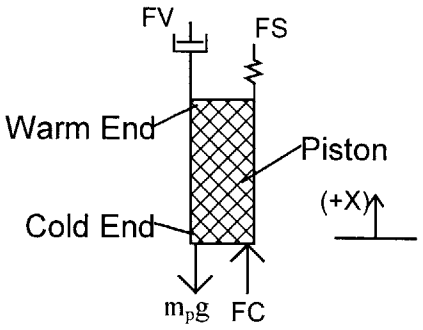

Figure 9: Free Body Diagram of Piston

all the forces that acted on the piston during the blow-in process, were represented. FC represented the pressure force in the cold region of the expander.

$$FC = P_{in} \cdot A_c$$

Eqt 18

In equation 18, A_c represented the cross-sectional area of the piston and P_{in} represented the high-pressure inlet line pressure. The loading of the piston was not modeled as an instantaneous process. Instead, the loading was modeled using an exponential function with a time constant, shown in equation 19.

$$FC = C \cdot \left(1 - e^{\frac{-t}{\tau}}\right)$$

Eqt 19

In equation 19, C represented the steady-state loading of the piston.

Recall that in the blow-in process, it was assumed that no mass left the compressed warm region, and as a result, there was a gas spring in the warm region. The resulting force from the gas spring, equation 20, was modeled as a linear spring with K being the effective spring constant.

$$FS = K \cdot X$$

Eqt 20

To obtain a relation for the spring constant, the second law of thermodynamics was employed. Consider the form of the second law where s(V,P), equation 21.

$$-C_p \cdot \frac{d(A_c \cdot X)}{V} = C_v \cdot \frac{d\left(\frac{FS}{A_c}\right)}{P}$$

Eqt 21

Equation 21 was then rearranged to yield the effective spring constant, K, shown in equation 22. In equation 22, H represented the height of the region occupied by the gas in the warm region.

$$K = \frac{-d(FS)}{d(X)} = \frac{k \cdot P_g \cdot A_c}{H}$$

Eqt 22

In Figure 9, the dampening force, FV, was modeled two different ways. First, FV represented the shear stress caused by the thin layer of working fluid between the piston and the cylinder wall, equation 23.

$$FV = \frac{\mu \cdot A_s}{G} \cdot \frac{d(X)}{d(t)}$$

Eqt 23

In equation 23, G represented the radial distance between the piston and cylinder wall, and A_s represented the surface area of the piston. Since the shear stress did not provide adequate dampening, FV was then modeled a second way to represent the effect of the orifice. For a fist order analysis, Bernouli's equation for steady state incompressible flow was used to obtain a relation between the warm-end pressure, velocity of the piston and the cross-sectional area to orifice area ratio, A_c / A_o. Equation 24 shows the result of this model.

$$P(t) = P_{\infty} + \frac{1}{2} \cdot \rho \cdot \left(\frac{d(X)}{d(t)} \right)^2 \cdot \left[\left(\frac{A_c}{A_o} \right)^2 - 1 \right]$$

Eqt 24

To ensure a linear differential equation, the squared velocity term in equation 24 was approximated with only a first order velocity term by dropping the square.

The resulting governing equations of motion for the two different models are shown below in equation 25 and 26, respectively.

$$\frac{d^2}{dt^2} X + \frac{\mu \cdot A_s}{m_p \cdot G} \cdot \frac{d}{dt} X + \frac{k \cdot A_c \cdot P_{\infty}}{m_p \cdot H} \cdot X = \frac{P_{in} \cdot A_c}{m_p} - g$$

Eqt 25

$$\frac{d^2}{dt^2} X + \frac{1}{2} \cdot \frac{\rho}{m_p} \cdot \left[\left(\frac{A_c}{A_o} \right)^2 - 1 \right] \cdot A_c \cdot \frac{d}{dt} X + \frac{k \cdot A_c \cdot P_{\infty}}{m_p \cdot H} \cdot X = \frac{P_{in} \cdot A_c}{m_p} - g$$

Eqt 26

In order to solve these second order ordinary differential equations, algebraic substitutions were made to arrange equation 25 and 26 into the form of equation 27, where C represented the steady-state loading of the piston in equation 26 and 27.

$$\frac{d^2}{dt^2} X + 2\cdot\beta\cdot\frac{d}{dt}X + \omega_o{}^2\cdot X = C\cdot\left(1 - e^{\frac{-t}{\tau}}\right)$$

Eqt 27

The boundary conditions for the two differential equations were the same, $X(t=0)=0$ and $X'(t=0)=0$

To obtain a solution to the initial-value problem, the Laplace transformation method was employed. Taking the Laplace transform of equation 27, and solving for $L[X(t)]$, yielded the function shown in equation 28.

$$L(X(t)) = \frac{C}{\tau\cdot(s)\cdot\left(s+\frac{1}{\tau}\right)\cdot\left(s^2 + 2\cdot\beta\cdot s + \omega_o{}^2\right)}$$

Eqt 28

The next step, involved taking the inverse Laplace transform of equation 28 by use of contour integration. The result of the integration is shown in equations 29 and 30, and Figure 10 illustrated the contour in the s-domain, which was integrated.

$$X(t) = \frac{C}{\beta^2 + \omega 1^2} + \frac{-C\cdot e^{\frac{-t}{\tau}}}{\left(-\frac{1}{\tau}+\beta\right)^2 + \omega 1^2} + \frac{C\cdot e^{-\beta\cdot t}}{\tau\cdot\omega 1}\cdot\frac{\left(\beta^2 - \omega 1^2 - \frac{\beta}{\tau}\right)\cdot\sin(\omega 1\cdot t) + \omega 1\cdot\left(2\cdot\beta - \frac{1}{\tau}\right)\cdot\cos(\omega 1\cdot t)}{\left(\beta^2 - \omega 1^2 - \frac{\beta}{\tau}\right)^2 + \left[\omega 1\cdot\left(2\cdot\beta - \frac{1}{\tau}\right)\right]^2}$$

Eqt 29

$$\omega 1 = \sqrt{\omega_o{}^2 - \beta^2}$$

Eqt 30

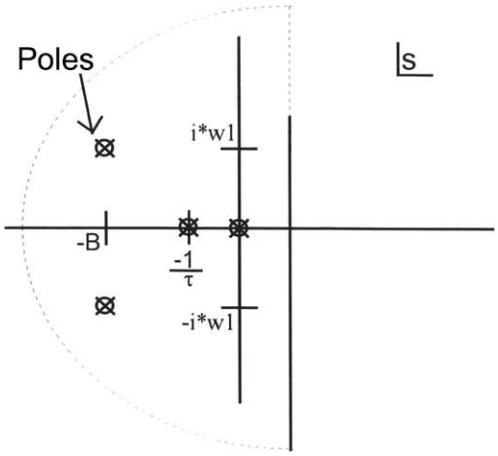

Figure 10: Contour Integration for Inverse Laplace Transform

These models for the dynamics of the piston, were used to investigate the vibration effects during the blow-in process. The results of this analysis were then used to determine if special consideration was needed in the control routine to monitor the rapid processes. It was equally important to ensure the system did not react uncontrollably to the sudden change in pressure and damage the testing apparatus. An example of the program used for the dynamic analysis is shown in Appendix F.

3 Design of Free-Piston Expander

3.1 Apparatus Design

Figure 11 illustrated a detailed sketch of the entire free-piston testing apparatus. The high-pressure Nitrogen line supplied the actuators and the pressure regulated working fluid to the expander. The Nitrogen, used as the working fluid, was regulated to remove any fluctuations in pressure that were present in the source line. In order to eliminate the flow restriction through the regulator, an inlet surge tank was placed between the regulator and the inlet valve. Since this experiment only consisted of a single stage apparatus, the exhaust line opened directly to the atmosphere.

The warm-end of the cylinder was mounted to a stationary stand through a split-ring and flange. A valve platform and brass cap, containing two throttles, were bolted to the top of the flange. The two throttles were soldered into the brass cap and connected to the 5/2-spool valve, which determined the intermediate pressure tank that was in communication with the warm end of the expander. The pressure tanks, constructed from gas cylinders, were connected to the system through 3/8" copper tubing.

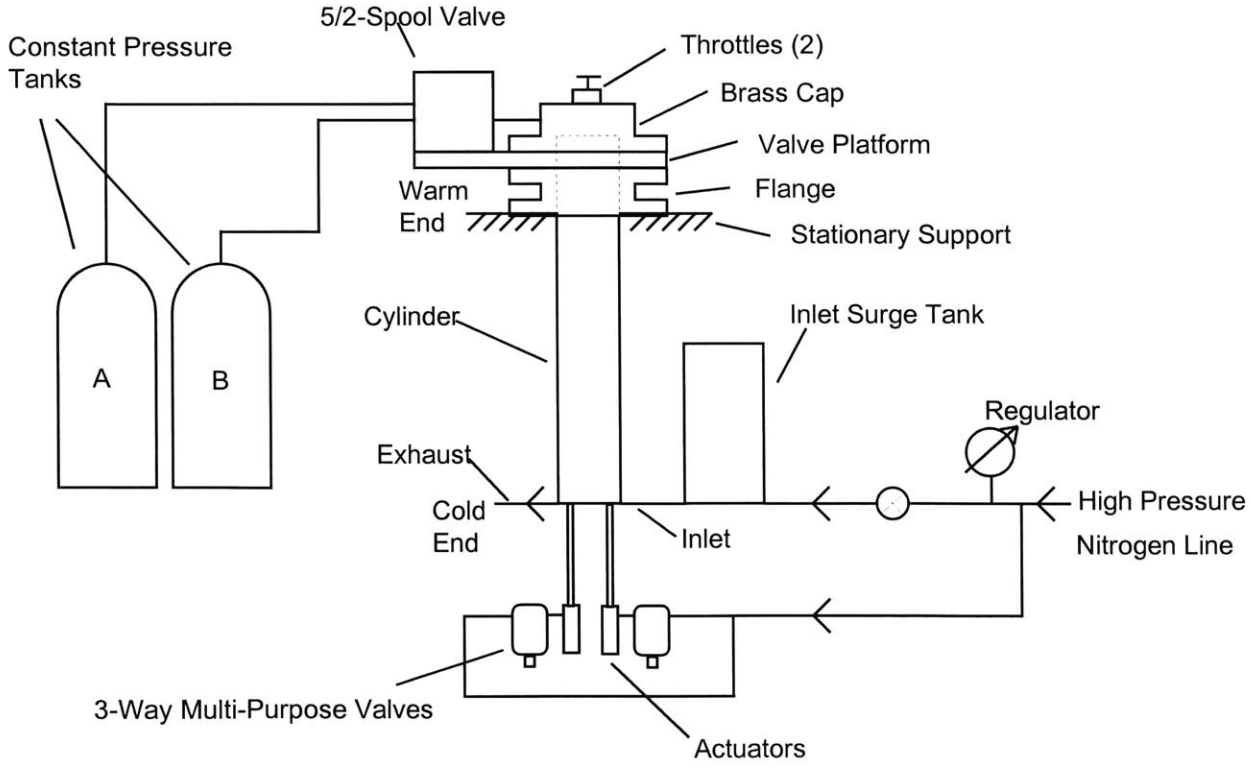

Figure 11: Detailed Sketch of Free-Piston Testing Apparatus

In Figure 11, the cylinder, inlet valve, exhaust valve and inlet surge tank were employed from a previous experiment by Ludwigsen. Design and constuction of the free-piston apparatus focused on the warm-end of the expander and control of the cyclic operation.

3.1.1 Valves

In the free-piston design, the valve sizes and sequencing were critical to control of the expander. the throttle valves, responsible for dissipating the work, were the most critical valve in the design of the apparatus. An angled needle valve, made by Whitey, model B-1RM4-A, was chosen for two reasons. First, using the correlation in equation 31, provided by Minuteman Controls Co., it was determined that a flow factor of Cv=.05 was needed to run test at one Hz, the cyclic frequency for testing.

$$Cv = \frac{1.024 \cdot Q}{\sqrt{(P_2 - P1) \cdot (P_2 + 14.7)}}$$

Eqt 31

These needle valves had an approximately linear, Cv verses turns opened, relationship in the range of flow restrictions required for testing. The second factor in choosing these valves involved minimizing the void space when the piston was at top dead center. As shown in Figure 13, the bottom portions of the needle valves were machined flat except for a lip used to index the position of the valves. When the valves were then mounted in the brass cap, as shown in Figure 14, this allowed the valve seats to rest directly above the cylinder, minimizing the void space between the piston and the orifice. A list of parts for Figure 13 through Figure 15 was located in Table 1

The ROSS 5/2-spool valve, model W7016A2331, was used for controlling flow between the throttle valves and the intermediate pressure tanks. This valve allowed for two configurations of testing, illustrated in Figure 12. Configuration (I) used one of the throttle valves, and sealed ports one and three. Toggling the solenoid on and off selected the intermediate pressure tank, which was connected to the warm end through throttle 1. Configuration (II) employed two throttles, and only port four was sealed. Testing in this configuration allowed the throttling into each of the pressure tanks to be controlled independently. As configuration (II) illustrated in Figure 12, throttle 1 controlled the gas flow into tank A and throttle 2 controlled the gas flow into tank B. Although configuration (II) had no effect on the thermodynamic model, it provided variable control of the dynamics of the cycle.

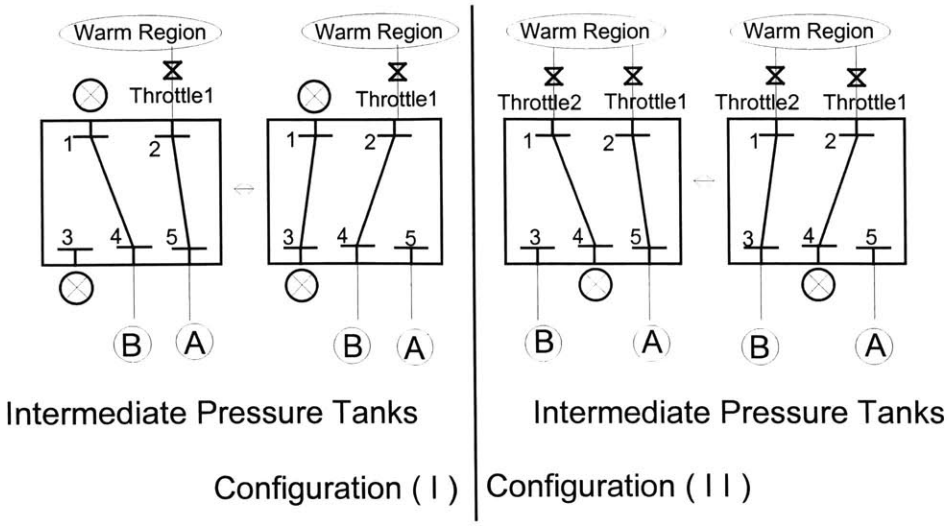

Figure 12: Spool Valve Configurations

List of Parts(figures 13-15)		
Part #	Name	Notes
1	Brass Cap	Brass
2	Cylinder	Stainless Steel
3	Flange	Stainless Steel
4	O-Ring	Rubber
5	Split-Ring	Stainless Steel
6	Throttle	Brass
7	Valve Platform	Carbon Steel

Table 1: List of Parts for Figures 13-15

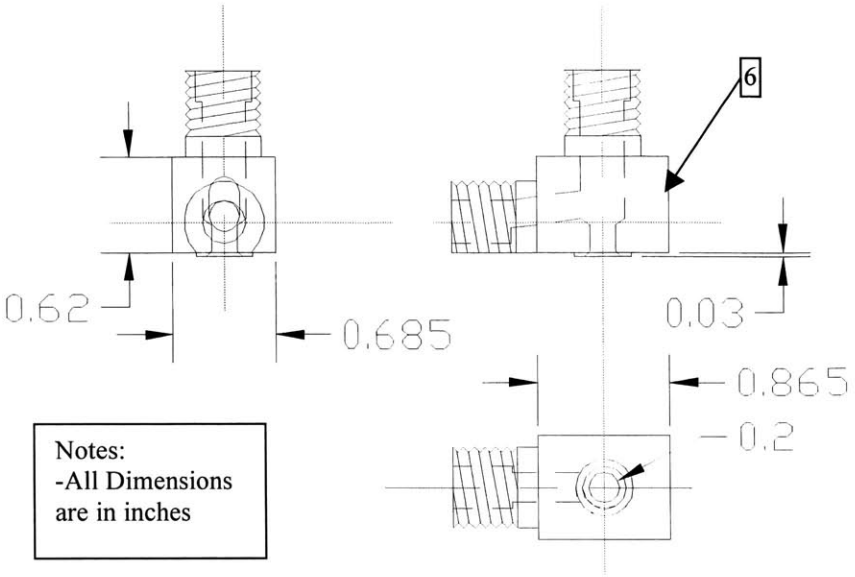

Figure 13: Machined Throttle Valves

3.1.2 Flange

As shown in Figure 11, the testing apparatus was suspended from a stationary support. To mount the apparatus, the flange, which bolted to a testing stand, held a split ring in place around the cylinder, Figure 15. With the flange attached to the testing stand, it became the stationary point to which the valve platform and brass cap were bolted. The clearance holes for the bolts can be seen in both Figure 14 and Figure 15.

3.1.3 Brass Cap

One of the most critical components in the warm end assembly was the brass cap. The cap had to be machined in such a manner as to minimize the void space in the cylinder at top dead center and provide a static seal for the warm end of the expander. Figure 15 showed the relative position of the two throttles to the top of the cylinder. The throttles were soft soldered to the brass cap and a support plate was screwed down on top of the valves to provide extra stability. As illustrated, the seats on the throttles rested just above the top dead center position of the cylinder. This minimized the void space above the piston at state 4 of the cycle.

The brass cap also provided a static seal for the warm end of the expander. As illustrated in Figure 15, the outside of the cylinder was turned to allow for a 1/8", male gland, o-ring. This o-ring provided a static seal to the inside bore of the brass cap when the cap was securely bolted to the flange.

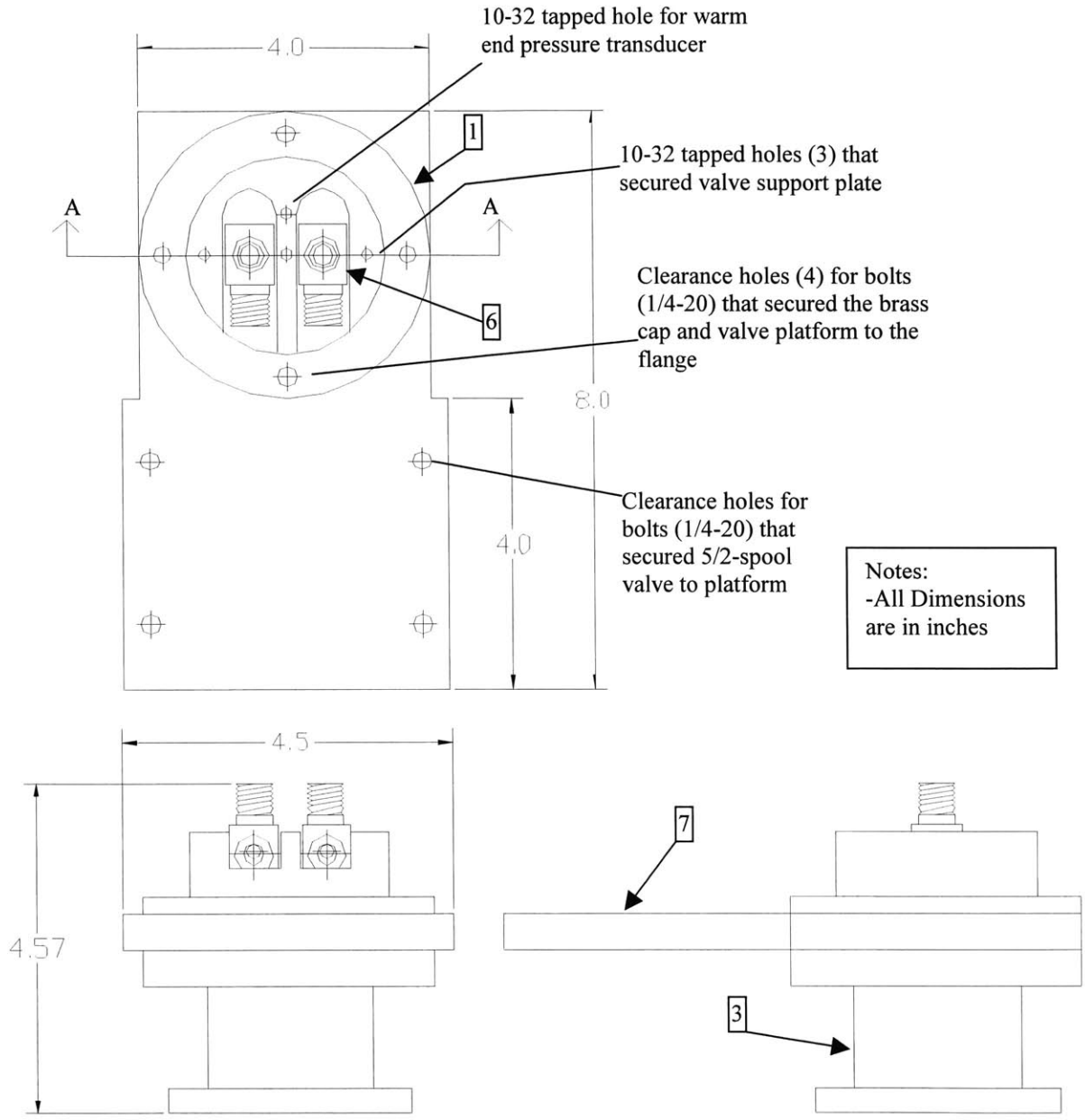

Figure 14: Warm-End Assembly

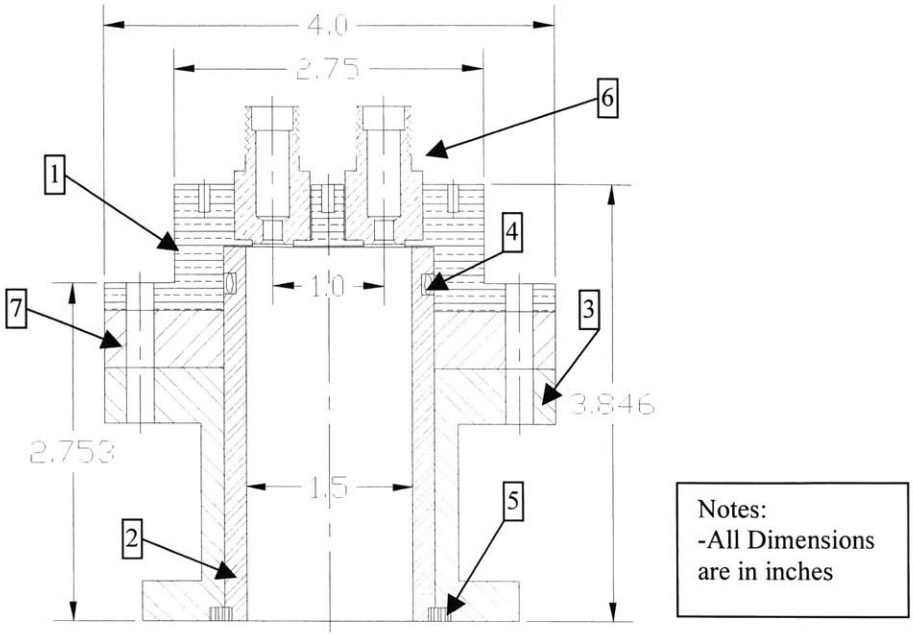

Figure 15: Assembly Cross-Section View A-A

3.1.4 Piston

The piston was constructed from a G-10, thin-walled, cylinder filled with foam, and the ends of the piston were attached using STYCast 1266 epoxy encapsulate. There were three main considerations for the piston design. First, the length of the piston was chosen to be 35.485" in length, which resulted in a 1.528" stroke. The piston was then turned down to a final diameter of 1.492", which determined the clearance between the piston and cylinder wall to be .008". The clearance needed to be small enough to restrict the flow around the outside of the piston during the expansion process, but not too small that the errors in both the cylinder and piston would result in drag between the cylinder wall and piston.

The final consideration for the piston is illustrated in Figure 16. Although there were no physical connections to the piston, its exact position and velocity were critical to the control routine.

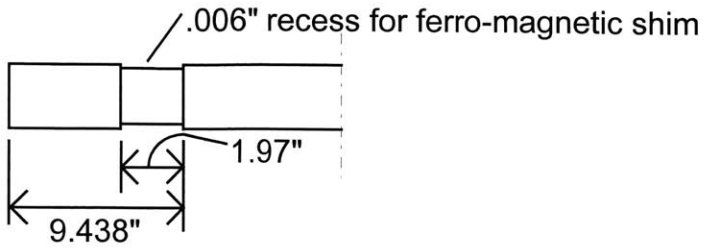

Figure 16: Warm End Sketch of Piston

To determine the position of the piston, a linear variable differential transformer (LVDT) was designed and integrated into the piston and cylinder. A ferro-magnetic steel shim (.002" thick) was epoxied into the machined recess on the piston wall, illustrated in Figure 16. The operation of the LVDT will be discussed in section 3.2.1.

3.2 Instrumentation and Signal Conditioning

Instrumentation for the free-piston apparatus was required for two reasons. First, data needed to be collected and compared with the optimized models to analyze the performance of the expander. More importantly, it was necessary to monitor the status of the expander to provide information to the control routine. It was essential that the pressure in the expander and position of the piston were monitored adequately to provide information about the transient behavior of the system. Although the thermal performance of the system was not a focus of the experiment, temperature measurements for the inlet and exhaust lines were also obtained.

3.2.1 Linear Variable Differential Transformer

To detect the position of the piston, a LVDT was designed and integrated into the cylinder and piston. Figure 17 provided a cross-sectional view of the LVDT as it was mounted on the apparatus. The Inductance coils were wound around the warm-end of the thin-walled cylinder. The windings formed two double-layer coils with a center tap between the two coils. An AC excitation voltage, shown as v_{in} in Figure 17, was applied across the full length of the two coils, and the output voltage, v_{out}, determined the position of the piston inside the expander. Equation 32 illustrates that the output voltage from the LVDT was in phase with the excitation voltage and the magnitude was controlled by the relative inductance of the two coils.

$$v_{out} = \frac{v_{in} \cdot L2}{L1 + L2} \cdot \cos(\omega \cdot t)$$

Eqt 32

V_{in} and ω were the amplitude and frequency of the excitation voltage, respectively. L1 and L2 were the respective inductance values for the two coils.

The inductance of the two coils was varied by the location of the steal shim epoxied to the piston.

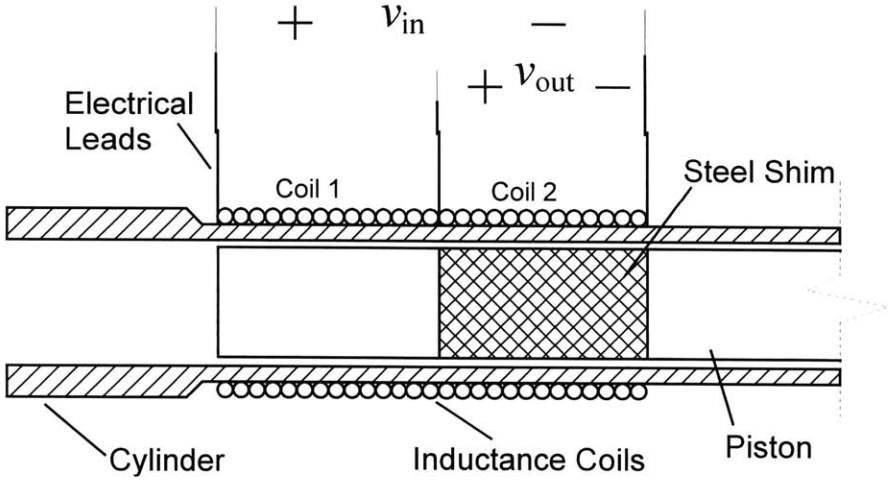

Figure 17: Cross-Sectional View of LVDT

The inductance of each individual coil was increased as the shim entered the core of that coil. The steal shim was mounted on the piston, relative to the pick-up coils, such that the output signal from the LVDT was in the linear range for the given stroke length. Calibration curves for all of the instrumentation can be found in Appendix C.

The output signal from the LVDT was conditioned using the circuit illustrated in Figure 18. The bridge consisted of the two coils wound on the outside of the cylinder. The coils were in parallel with an adjustable ratio transformer. The parallel coils and transformer formed the two legs of an inductance bridge. The ratio transformer allowed precision adjustments in the inductance ratios to balance the bridge. Even with the bridge balanced, the AC output signal was not compatible with data acquisition system. It was necessary to convert the 6 KHz AC signal to a DC signal that would vary with the position of the piston. To achieve this conversion, a lock-in amplifier was employed. The amplifier in Figure 18 multiplied the reference signal and input signal together to yield equation 33. V_{ref} and v_{input} were the respective amplitudes and α represented the phase shift of the input signal with respect to the reference signal.

$$\frac{V_{input} \cdot V_{ref}}{2} \cdot (\cos(2 \cdot \omega \cdot t + \alpha) + \cos(\alpha))$$

Eqt 33

Passing this result through a low-pass filter, the amplifier then output the signal represented by equation 34.

$$\frac{V_{input} \cdot V_{ref}}{2} \cdot (\cos(\alpha))$$

Eqt 34

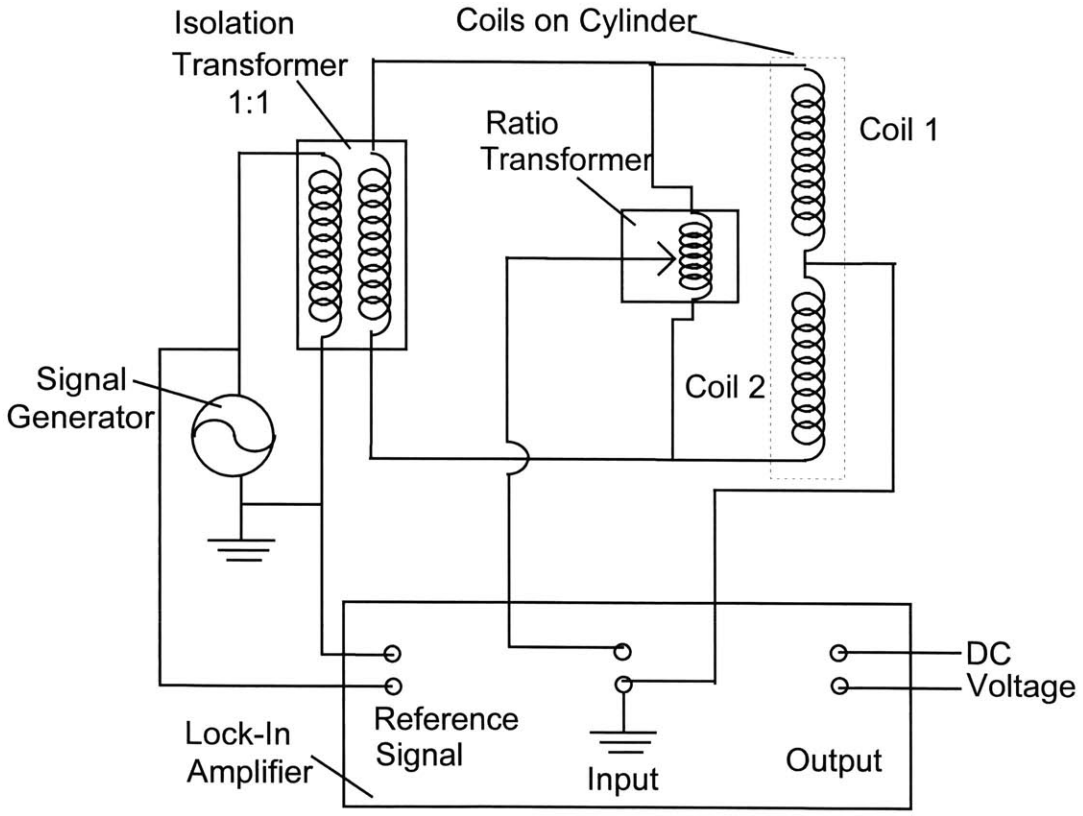

Figure 18: LVDT Electrical Schematic

Consider a balanced bridge in Figure 18 with the shim center between the two coils, if the ferro-magnetic core entered coil 2, the input signal to the amplifier became negative and was 180 degrees out of phase with the reference signal. As the steel core moved back to the center of the two coils, the magnitude of the negative DC output signal decreased to zero. The two signals were then in phase as the core passed into coil 1, producing a

positive DC signal proportional to the position of the piston. The 1:1 isolation transformer was used to eliminate a ground loop since both the signal generator and an input signal terminal were grounded.

3.2.2 Pressure

Both static and dynamic pressure conditions were monitored throughout the apparatus. Static pressure measurements were obtained manually from gauges on the regulated inlet line and the intermediate pressure tanks. These locations in the system were maintained at constant pressure and were not needed for the control routine. However, the transient behavior of the pressure inside the expander was required in the control routine.

In the warm region, an ENDEVCO strain gauge pressure transducer, model AG497, was threaded into a pressure tap machined in the brass cap. The signal from this transducer was routed through an ENDEVCO, model 4428A, pressure indicator which had a five volt F.S.O. The transient pressure in the cold region of the expander was monitored by a KISTLER, model 603B3, piezo-quartz pressure transducer. The signal was then processed in a KISTLER, model 5004, charge amplifier with a ±10 volt F.S.O.

3.2.3 Temperature

Although the focus of the experiment was not the actual cooling of the working fluid, temperature measurements for both the inlet and exhaust lines were acquired by the data acquisition system. Type E, chromel and constantan, thermocouples were used along with their appropriate cold-junction compensator units. The inlet thermocouple was soldered into a tube fitting, which was mounted on the lower end of the inlet surge tank. The exhaust line thermocouple was placed in the flow of the exhaust gases. Since the exhaust line was opened to the atmosphere, transient behavior in the temperature was observed between the surge of exhaust gas and the exhaust line being back-filled with atmospheric gases. An average over several cycles was used to eliminate these fluctuations in data.

3.3 Control Design

The free-piston expander was monitored with a DAS-20 data acquisition board, manufactured by Keithley MetraByte Corporation. The DAS-20 monitored the two pressure transducers, two thermocouples and the LVDT. The digital output from the DAS-20 controlled the inlet and exhaust valves along with the 5/2-spool valve on the warm end of the expander.

The control program, written in QBasic 4.5, utilized pre-defined, machine language, call routines to perform all I/O operations. All required calculations to control the system were performed within the QBasic program. The program, shown in Appendix D, was divided into a manual mode and an automatic mode, which provided complete control of the expander and data storage.

The manual mode served two purposes. First, the manual mode was used to initialize the system for cyclic operation and troubleshoot any problems in the system. Second, this mode was used to transfer data from Basic arrays, acquired during automatic operation, to disk for manipulation. The six permissible operations in this mode are shown in Table 2.

KEY PRESS	OPERATION
I	Toggle inlet valve opened/closed
E	Toggle exhaust valve opened/closed
T	Toggle 5/2-Spool Valve
A	Write QBasic data array to A:\ drive
B	Begin automatic operation
X	Terminate program and return to code

Table 2: Options in Manual Mode

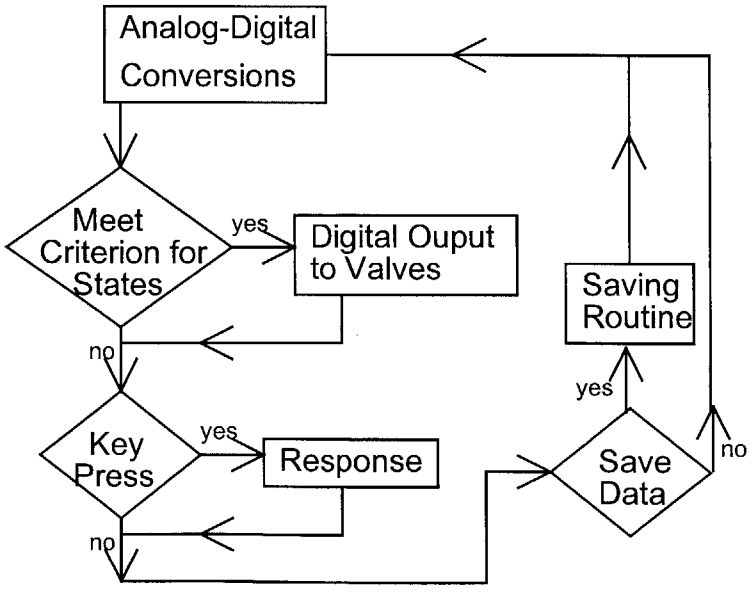

Figure 19: Flowchart for Automatic Mode

The automatic mode, illustrated in Figure 19, involved sampling data, determining the appropriate response and saving the data for manipulation. The sampling rate of the data needed to fast enough to capture the transient behavior. However, if the DAS-20 sampled the data too fast, an overload of data points during the slower processes of the expander would affect the system's ability to determine the correct state. Programming adjustable wait loops throughout the program, allowed the sampling rate to be controlled for most scenarios. All input signals being sampled, were sufficiently amplified with the DAS-20 on-board amplifiers.

After the data was sampled, it was necessary to determine the state of the expander and what action, if any, was required. As labeled in Table 3, certain states required a specific action from the control routine.

STATE	ACTION
2	Close inlet valve
3	Toggle 5/2-Spool Valve
4	Open exhaust valve
6	Close exhaust valve
7	Toggle 5/2-Spool Valve
8	Open inlet valve

Table 3: Valve Control for States in Cylce

The digital output signals used to control the appropriate valves were routed to optical relay switches that provided power to actuate the valves.

The control routine logic used during automatic operation to determine the states of the cycle was illustrated in Figure 20. In the program, all rate values were determined by comparison of the current data set with the previous data set, and V^*_2 was a preset value in the program. When the program was distinguishing between states 3 and 4 or states 6, 7 and 8, the signals on the digital output channels were sampled to determine the previous output signal and the appropriate new signal. If the sampled data passed all the checks in Figure 20 and did not match one of the pre-defined states, the expander was in an undefined situation. The system was consequently shut down automatically to prevent an incorrect switch that could damage the system.

The automatic mode also allowed limited user interface, Table 4. Control of the preset value for V^*_2 was given to the user, rather than optimized by the program. This allowed experiments to be run for unmatched strokes.

The user was also able to determine when the program would save the data sets to arrays. When the "W" key was pressed, the program saved a preset number of data sets, which covered several cycles and provided adequate resolution for each cycle. To streamline the program, only the raw A/D signals were saved to the arrays. Data manipulation and curve fitting was handled by the separate data manipulation worksheet, shown in Appendix E.

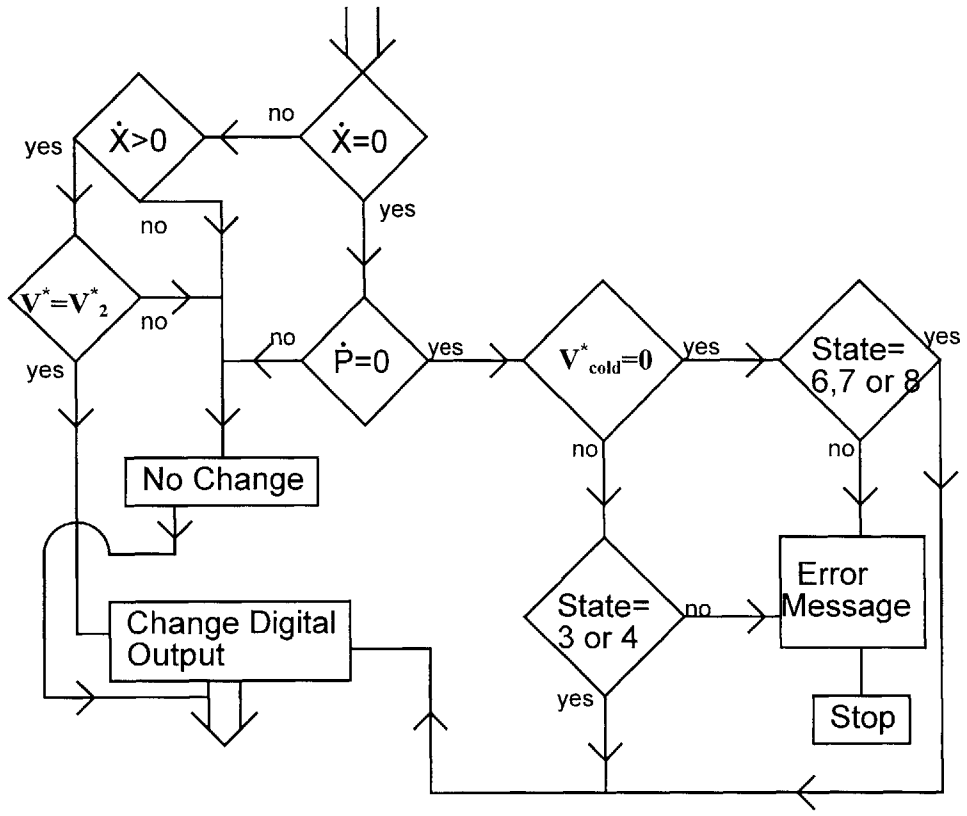

Figure 20: Logic to Determine Sates in Cycle

KEY PRESS	OPERATION
U	Increase V^*_2
D	Decrease V^*_2
W	Write data to Basic Array
S	Stop automatic operation

Table 4: User Options in Automatic Mode

4 Results

4.1 Optimization

4.1.1 Rubber Geometry

The first model optimized was the rubber geometry model, in which the pressures and volume matched at top dead center. The first analysis of this model used normalized equations programmed into a spreadsheet to obtain the steady-state cyclic conditions. The optimum solution, for a given P^*_{out} and T^*_{∞}, was obtained by varying P^*_A, P^*_B and V^*_2 until a steady-state solution, with T^*_{out} minimized, was obtained. Figure 21 illustrated the optimum solution for a rubber geometry scenario with P^*_{out} equal to one tenth.

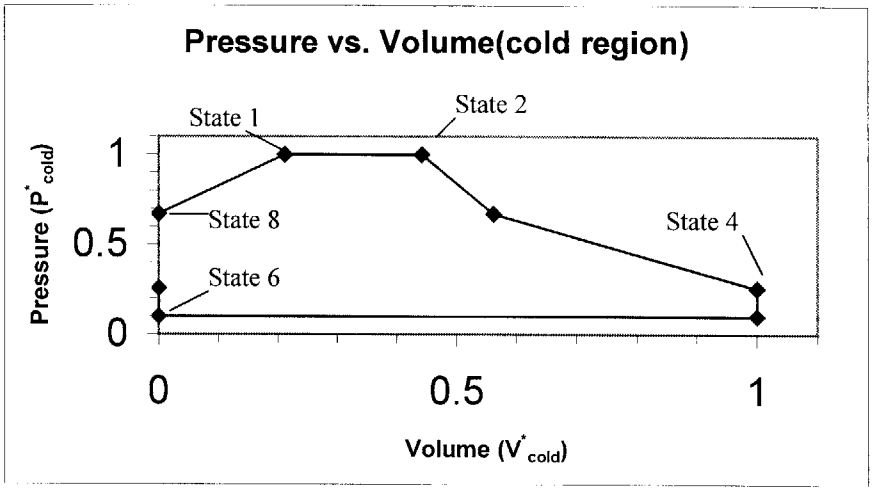

Figure 21:, P^*_{cold} -V^*_{cold} diagram for Matched Stroke

When Figure 21 was compared to Figure 2, there were several differences. First, the optimizing routine only provided information about the equilibrium states and did not provide information between the states, resulting in the piece-wise plot. Consequently, the isentropic expansion and blow-in processes are not accurately represented. The isentropic expansion was a smooth quasi-static process while the experimental blow-in process closely resembled that of Figure 2 rather than Figure 21.

Figure 22 provided information about the temperature in the cold region of the expander during the cycle. This plot is not continuous because all of the working fluid was exhausted at state 6, and assigning a temperature to the cold region no longer had any meaning. Therefore, the temperature of the fluid at state 1 was independent of

the exhausted fluid's temperature. Notice that the fluid's temperature in the cold region at state 1 was slightly higher than that of the inlet line temperature. This increase in temperature was associated with the entropy generated due to the irreversibilities of the inlet valve. A similar loss was evident in the blow-down process from state 4 to state 5. The temperature of sub-system X, labeled in Figure 4, decreased more than that of sub-system Y. This was a result of concentrating all of the irreversibilities in the exit valve. In Figure 22, state 5 represented the temperature of sub-system Y, and state 6 was the mass weighted average of the two sub-systems in the exhaust line.

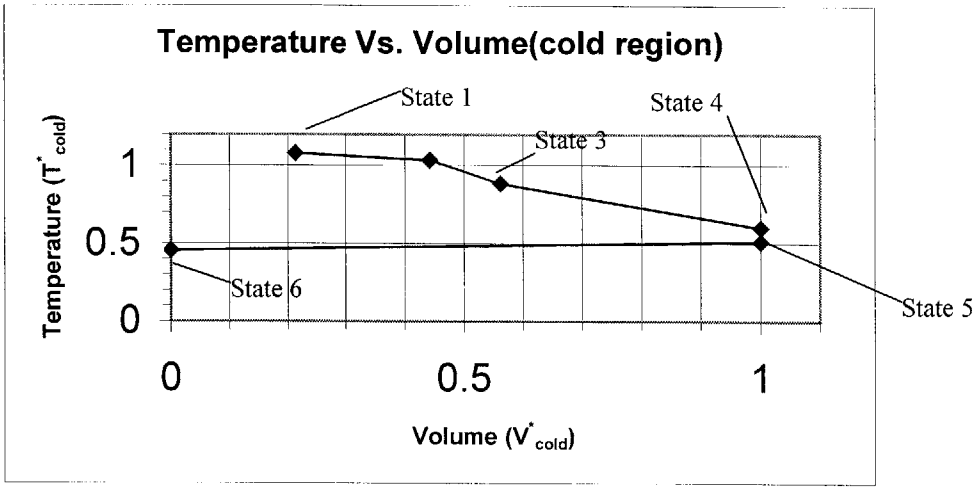

Figure 22:, T^*_{cold} -V^*_{cold} Diagram for Matched Stroke

The matched stroke scenario was optimized a second way. All of the equilibrium equations were combined to yield a single algebraic expression for the exhaust line temperature of the working fluid. Although the expression for the temperature was complex, it was optimized as a function of only V^*_2 because of the modeling assumptions discussed in section 2.3. The worksheet for this optimization is shown in Appendix B.

In the rubber geometry system, P^*_{out} and T^*_∞ were fixed and there was only one adjustable parameter: P^*_A, P^*_B, or V^*_2. These three parameters were not independent of each other. First, to ensure that the piston reached top dead center at the same time that the pressure in the warm region drop to P^*_B, V^*_2 and P^*_B were related through equation 35.

$$\frac{V_2}{V_{max}} = \left(\frac{P_B}{P_{in}}\right)^{\frac{1}{k}}$$

Eqt 35

The second condition, which held true for all models, was that the net flow of mass into the intermediate tanks must equal zero over one cycle. For the rubber geometry model with two tanks, this requirement was satisfied by equation 36.

$$\left[\left(k - 1 + \frac{P_A}{P_B}\right)\cdot\left[1 - \left(\frac{P_A}{P_B}\right)^{\frac{-1}{k}}\right] - 1 + -(k-1)\cdot\frac{P_{out}}{P_B}\right] = 0$$

Eqt 36

Figure 23 illustrated this mass balance requirement for a model where P^*_{out} equaled one tenth.

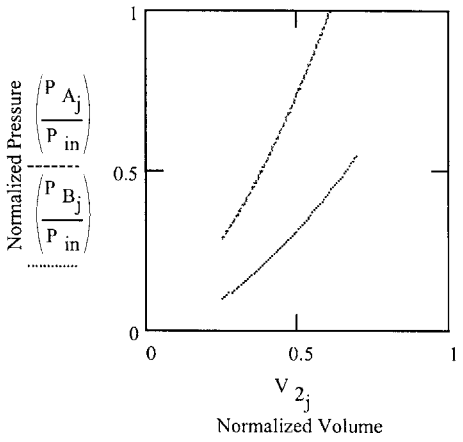

Figure 23: Equilibrium Intermediate Pressures for Rubber Geometry Model

With these two restrictions, the three adjustable variables were reduced to a single independent variable.

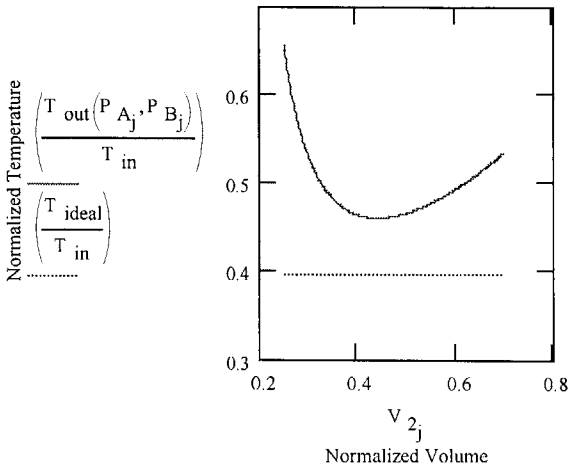

Figure 24: Optimized T^*_{out} for Rubber Geometry Model (P^*_{out}=.1)

Figure 24 demonstrated that there was a clear set of system parameters which provided optimum cooling of the working fluid. For the rubber geometry model, these parameters were P^*_A=.619, P^*_B=.257, and V^*_2=.442. These parameters produced an exhaust line temperature of T^*_{out}=.462, as compared to an isentropic expansion between the same P_{in} and P_{out} that produced T^*_{out}=.398.

The work transferred away from the cold region was rejected as heat in the warm end of the expander. The model of the expander system assumed all heat generated in the warm end was lost to the surrounding environment and that the intermediate pressure tanks were constant temperature. However, as the fluid was throttled back into the warm region during the charging process, state 6 though 8, the temperature increased as shown in Figure 25.

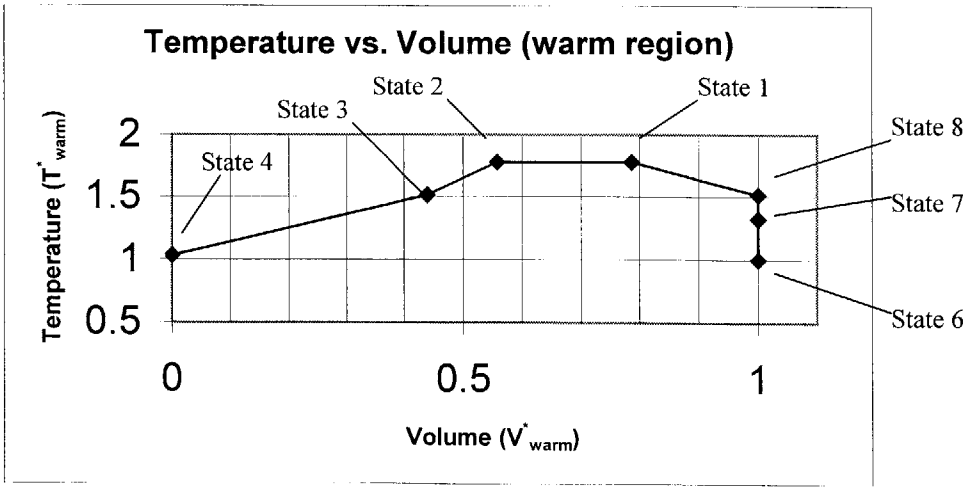

Figure 25:, T^*_{warm}-V^*_{warm} Diagram for Matched Stroke

For the rubber geometry model, the temperature at state 6 in the warm region of the expander was equal to the temperature of the surroundings. This was a direct result of the modeling assumption that there was zero void space in the warm region of the expander at state four.

The rubber geometry model was extended to systems with three and four intermediate pressure tanks as illustrated in the P^*_{cold}-V^*_{cold} plots of Figure 26 and Figure 27. In these models, the stroke always matched at top dead center as in the rubber geometry model. For the same P^*_{out}, T^*_{out} decreased with the number of intermediate pressure tanks. This decrease in T^*_{out} was a result of less loss during the blow-in and blow-down process. With more intermediate pressure tanks, the equilibrium pressure in the highest and lowest pressure tank approached the inlet and exhaust line pressures respectively.

The increased cooling with the multiple tank models only produced T^*_{out}=.43 and T^*_{out}=.41 respectively. This was not a significant increase in cooling, and more importantly, the setup with only two tanks provided ample testing to demonstrate and investigate the behavior of the free-piston expander. As a result, no experimental tests were conducted with more than two tanks.

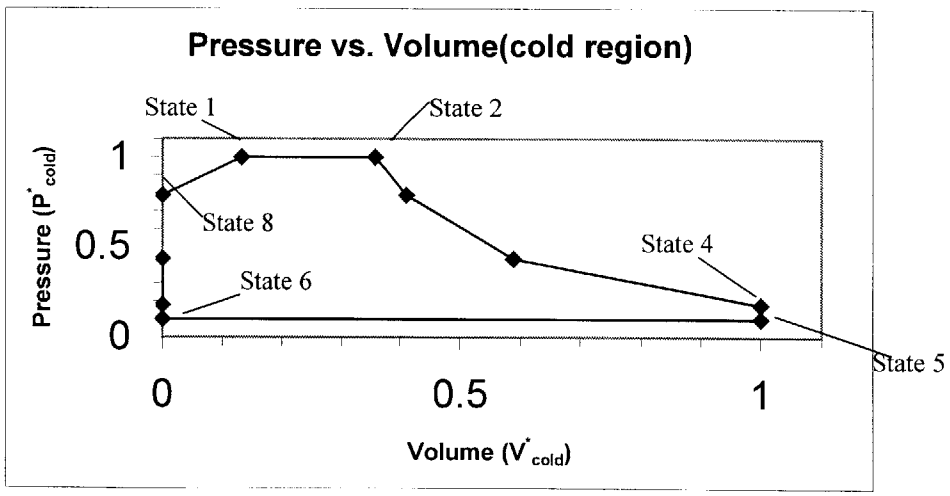

Figure 26: P^*_{cold} -V^*_{cold} Plot for Rubber Geometry Model with Three Pressure Tanks

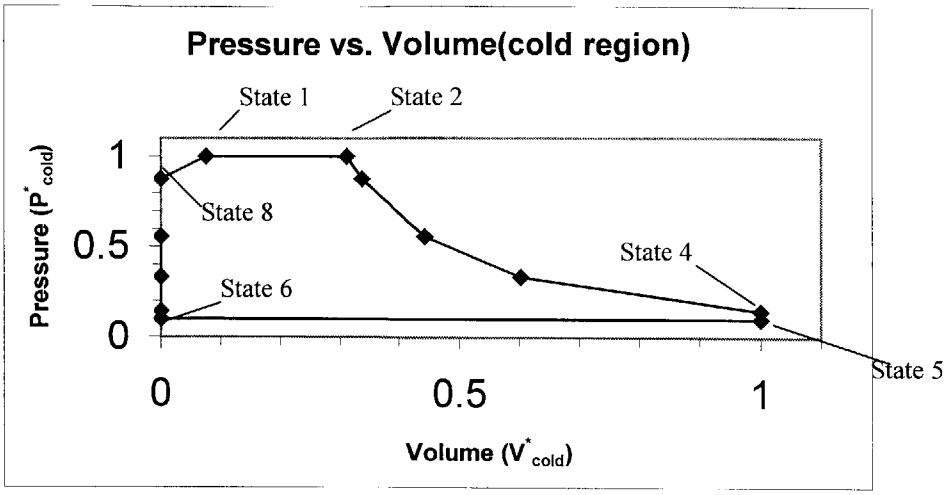

Figure 27: P^*_{cold} -V^*_{cold} Plot for Rubber Geometry Model with Four Pressure Tanks

4.1.2 Fixed Geometry

The next stage of analysis was the investigation of the actual system behavior with the fixed geometry model. The rubber geometry model involved many simplifying assumptions that needed to be addressed by determining the system's behavior when the final expansion stroke did not match at top dead center. In particular, the steady-state cyclic operating conditions of the fixed geometry models needed to be determined and optimized.

The first step was to determine if there existed an equilibrium set of system parameters for the fixed geometry model. To solve for these parameters, the modified modeling equations and constraints, developed in section 2.3.2, were programmed into a spreadsheet to obtain an iterative solution for the steady-state operating conditions. As in the rubber geometry model, the system's cycle was said to be in equilibrium when the net flow of mass into the intermediate pressure tanks equaled zero over one cycle. The program revealed multiple combinations of the intermediate pressures that satisfied this equilibrium condition for each value of V^*_2.

With the fixed geometry model predicting multiple steady-state operating conditions for each value of V^*_2, the next step was to determine the optimum set of operating parameters which produced the minimum T^*_{out}. To investigate the optimum behavior of the system, the low stroke and high stroke cases for the fixed geometry model were first considered separately and then together in conjunction with the rubber geometry model. Example P^*_{cold} vs. V^*_{cold} plots are shown in Figure 28 and Figure 29.

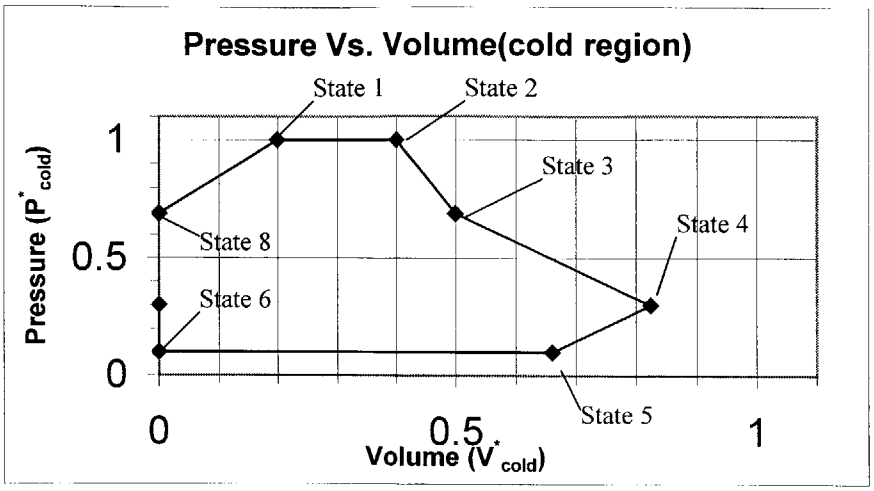

Figure 28: Low Stroke Cycle for Fixed Geometry Model

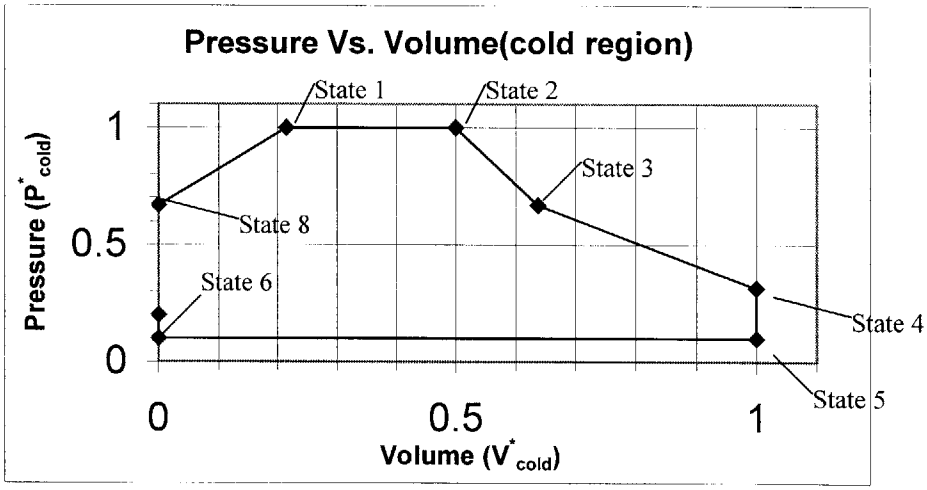

Figure 29: High Stroke Cycle for Fixed Geometry Model

For the fixed geometry model, it was neceassrary to determine if the piston was stopping on a low stroke or if the piston reached top dead center too soon in order to know which set of equations applied. Recalling that the expansions were all isentropic, equation 35 was used to determine which set of equations were needed. Rearranged in equation 37, it was shown that there was a critical value for $P^*_{B,}$ which was determined by the preset value of V^*_2.

$$P_B = P_{in}\left(\frac{V_2}{V_{max}}\right)^k$$

Eqt 37

If P^*_B dropped below this critical value, the piston reached top dead center too soon, and if the value of P^*_B was above this critical value, the stroke stopped short.

To illustrate the results of these programs, a value of .4 was chosen for V^*_2, and the equilibrium results for both of the unmatched cases are shown in Figure 30 and Figure 31. In these plots, P^*_B was used as the independent variable, and P^*_A was adjusted to satisfy the equilibrium constraint for the intermediate tanks. The normalized system parameters plotted as function of P^*_B were P^*_A, the high intermediate pressure, V^*_4, volume at state 4 in the cold region, and T^*_{out}, the final temperature of the exhaust line.

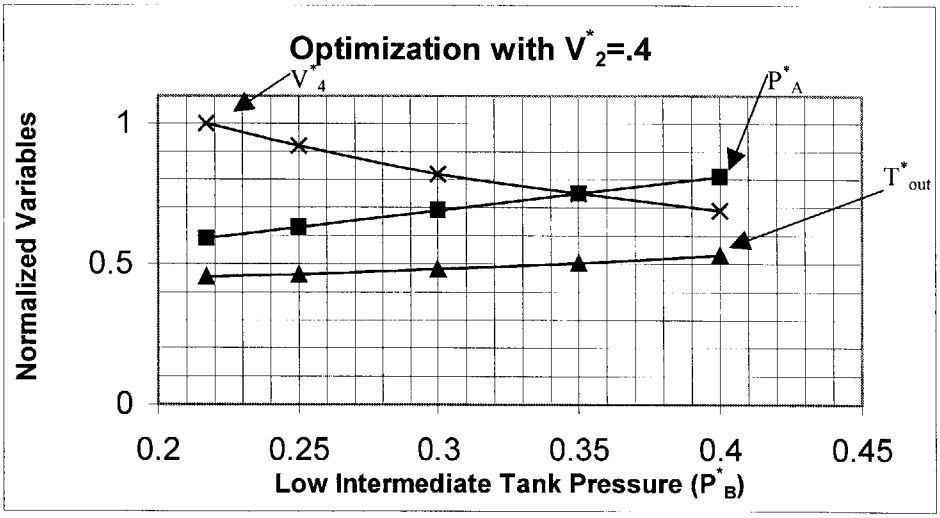

Figure 30: Low Stroke Optimization

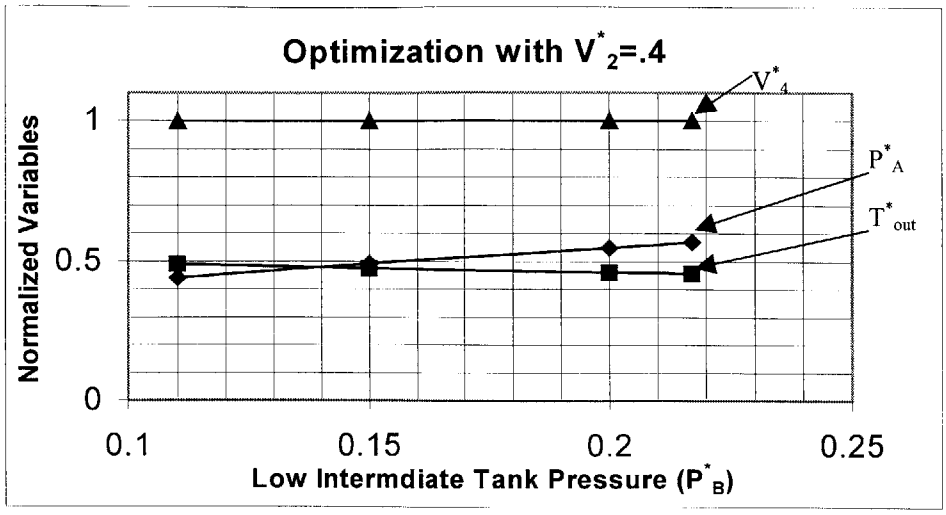

Figure 31: High Stroke Optimization

The spreadsheet model, which produced Figure 30, was only valid for cases in which $V^*_4<1$, or $P^*_b>(.22)$. Similarly, the model which produce Figure 31 was only valid for $V^*_4=1$, or $P^*_b<(.22)$. In both of these figures, it was clear that T^*_{out} decreased as the independent variable approached these limiting parameters. To illustrate the optimum results more directly, the two fixed geometry models and the rubber geometry model were combined into one plot for $V^*_2=.4$, Figure 32.

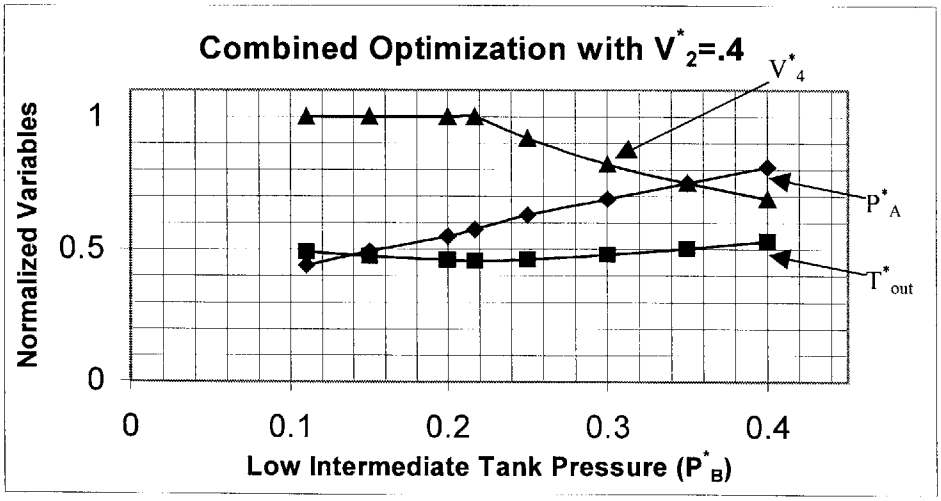

Figure 32: Combined Unmatched Optimization Results

Figure 32 showed that there was an optimum set of operating parameters, which coincided with that of the rubber geometry model. Consequently, the overall optimum operating conditions for the actual expander was the optimum set of parameters previously established for the rubber geometry model.

4.2 Dynamics

The dynamic analysis of the system consisted of two models for the blow-in process. First, the process was considered with the warm end sealed and only the viscous forces were responsible for vibrational dampening, which resulted in Figure 33. This result was based on a model with $P^*_A = (.8)$.

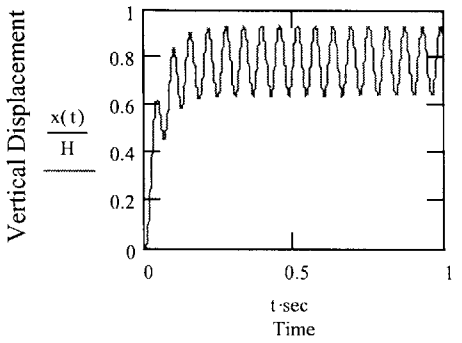

Figure 33: Blow-in Process with Only Viscous Dampening

The model showed that there was no significant dampening from the viscous forces and the piston oscillated over approximately two tenths of the total stroke. In the actual expander, the piston never reached a steady state oscillation due to the throttling effects in the warm end. Therefore, the model was modified to include the dampening effects of the throttle during the charging process.

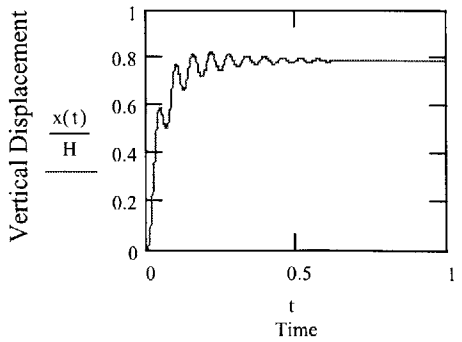

Figure 34: Blow-in Process with Throttling effects

Including the throttling effects, Figure 34 illustrated there was significant dampening during the blow-in process. However, the dampening was still minimal over the time of interest for the blow-in process because as the throttle valves were opened to allow more dampening the cyclic speed increased. Consequently, little dampening was evident during the experimental blow-in process. The effect of vibration in the system will be discussed in more detail with the experimental results.

4.3 Experimental

Although the modeling and optimization of the expander focused on the thermal performance, the experimental tests were conducted at room temperature with minimal insulation. The data collected was used to investigate the design limitations of the physical apparatus and the control routine. Of particular interest was the dynamic response of the piston during the rapid processes of the cycle and the control routine's ability to provide accurate, real-time control throughout the cycle. The pressure-volume relations in the warm and cold regions of the expander were recorded and compared with the ideal plots and results of the models discussed earlier. The model plots and experimental plots were used to predict the amount of work transferred away from the cold end of the expander over one cycle. The ideal work, predicted work and actual work transferred from the cold region were then compared to quantify the expander's performance. Multiple configurations of the system were tested to investigate the transient behavior of the system and the steady-state operating conditions.

Consistent with the modeling process, the experimental tests investigated the system's behavior when the piston's stroke was low, matched and high. To perform the initial tests, large intermediate pressure tanks were used to remove any transient behavior in the system. Consequently, if there was a net mass flow into or out of the tanks, it did not effect the pressure over numerous cycles. The transient behavior of the system will be discussed later.

The plots shown below illustrated the system's behavior when the stroke was low and the piston did not complete the full stroke of 1.528 in. Figure 35 through Figure 37 showed the time dependent plots of the V^*_{cold}, P^*_{warm} and P^*_{cold}, respectively.

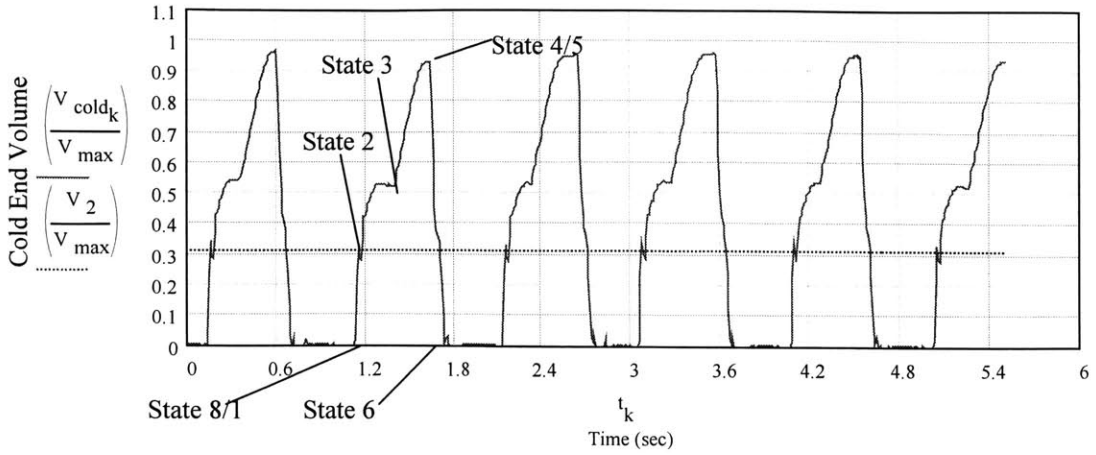

Figure 35: V^*_{cold} vs. Time for Low Stroke

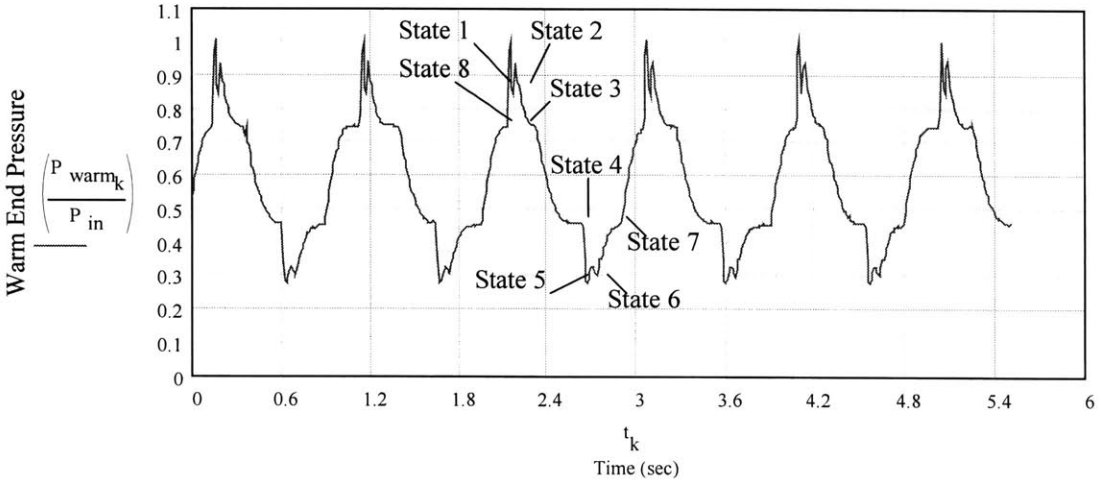

Figure 36: P^*_{warm} vs. Time for Low Stroke

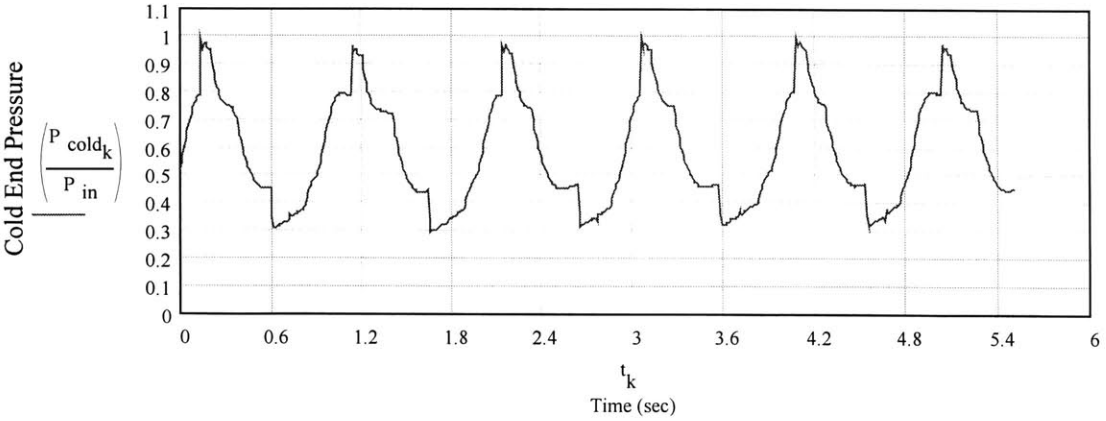

Figure 37: P^*_{cold} vs. Time for Low Stroke

In Figure 35, the straight line represented the volume corresponding to the preset value of V^*_2. One of the problems with the control routine was sensing this position and closing the inlet valve within a satisfactory range of this preset value. Because V^*_2 was reached during the blow-in process or close to the oscillation from the gas spring effect, this was the most inaccurate switch of the entire cycle. Figure 36 showed the pressure in the warm end of the expander as measured by the strain gauge transducer. The large oscillations in pressure, seen at the peak of each cycle, was generated by the oscillation of the piston during the blow-in process. The piezo-quartz transducer response, shown in Figure 37, was used in the cold region of the expander to obtain accurate measurements for the transient pressure. Although the piezo-quartz transducer's was ideal for rapid transients, it's signal drifted during the constant pressure processes. This drift in the signal could be seen during the charging process and during the exhaust stroke, when the pressure in the cold region of the expander was constant with time.

These three signals were needed to determine the state of the expander in the control routine, Figure 20. To determine if the rate processes in Figure 20 were equal to zero, the control routine compared two consecutive data points to see if they were within a certain range of each other. Figure 35 was used to determine if the velocity of the piston was zero, and Figure 36 and Figure 37 were used to determine when the pressure was constant. To determine the rate of change of pressure in the cold region during the blow-in process, data from the piezo-quartz transducer, Figure 37, was used because the strain gage transducer read the oscillations in the warm end. However, the control routine monitored the strain gage transducer, Figure 36, during the blow-down process because the piezo-quartz transducer exhibited too much drift over this constant pressure process.

Although these time dependent plots provided critical information to the control routine, they did not relate well to the results obtained from the optimization routines. Figure 38 and Figure 39 provided a better comparison for analyzing the expander's performance.

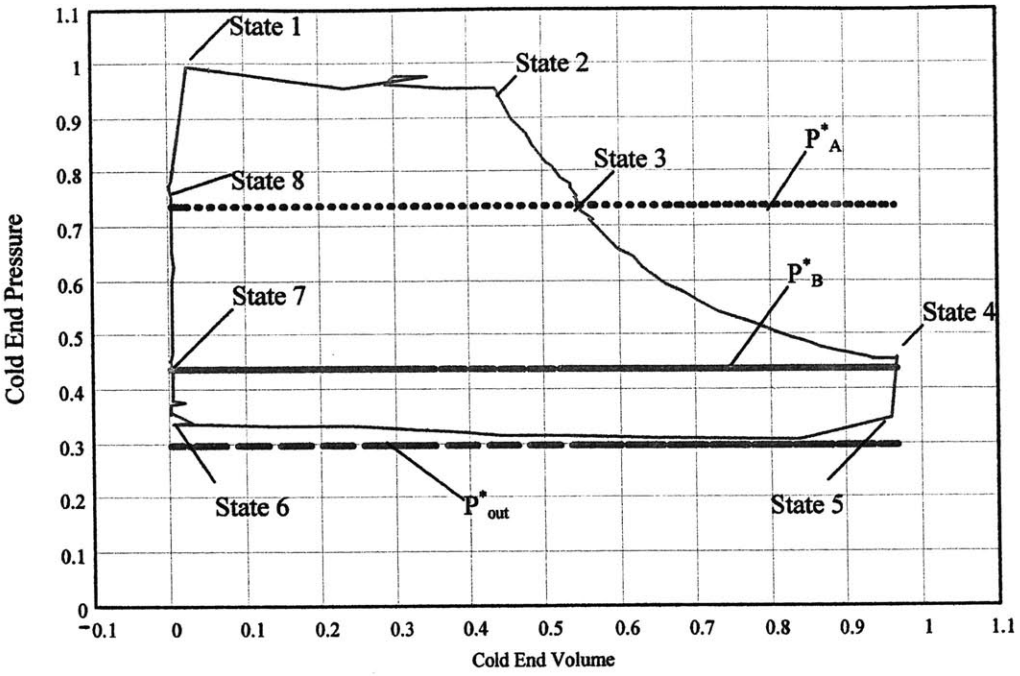

Figure 38: P^*_{cold} vs. V^*_{cold} Plot for Low Stroke

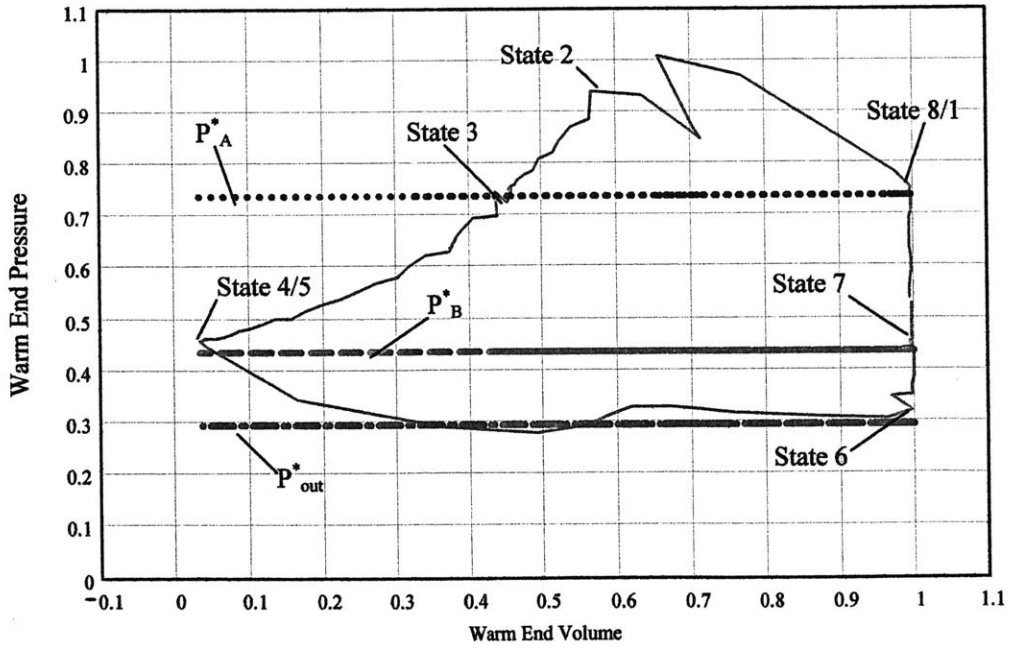

Figure 39: P^*_{warm} vs. V^*_{warm} Plot for Low Stroke

Notice the pressure-volume relation in Figure 38 looked more like the ideal plot of Figure 8, rather than the model results of Figure 28. During the blow-in process, the pressure in the cold region reached P^*_{in} before there was significant motion of the piston. In contrast, the warm region pressure increased as a result of the piston rising and compressing the fluid. It was difficult to obtain an adequate amount of data points during this rapid process to accurately represent the system's behavior. If the data acquisition's sampling rate was increased, the control routine mistook the relatively slower processes in the cycle as stalled and made incorrect switches. This lack of sufficient data points, which gave the plots a piece-wise appearance, could also be seen during the blow-down process in Figure 38 and Figure 39.

The drift, associated with the piezo-quartz transducer, was again evident in Figure 38 during the charging and exhaust process. The drift can also be seen at state 4 in the cycle when the pressure appears to slightly increase. Consequently, the pressure in the cold region of the expander was represented incorrectly in the plots for portions of the cycle.

To obtain a quantitative comparison between the ideal model, spreadsheet model and experimental results, the work represented by the P^*_{cold}-V^*_{cold} plot of each case was computed and tabulated.

	Ideal Model	Optimized Model	Experimental (cold region)
Work Computed (in-lb)	59.4	43	57.4
Normalized Work (W^*)	1	.72	.96

Table 5: Work Results for Low Stroke

The large discrepancy in Table 5 for the optimized model was largely due to the misrepresentation of the blow-in and blow-down processes as seen in Figure 28. Although the work computed for the experimental case was close to the ideal, the value should have been closer if the drift in the piezo-quartz transducer had been removed.

The next scenario, illustrated by Figure 40 through Figure 44, represented the apparatus when the stroke was matched. In Figure 40, the piston reached top dead center and remained there briefly during the blow-down process due to the minimized void space. The same issues discussed for the time dependent plots of the low stroke example can also be seen in the matched stroke results. In particular, the vibration of the piston and the drift in the piezo-quartz transducer are evident in the pressure verses time plots.

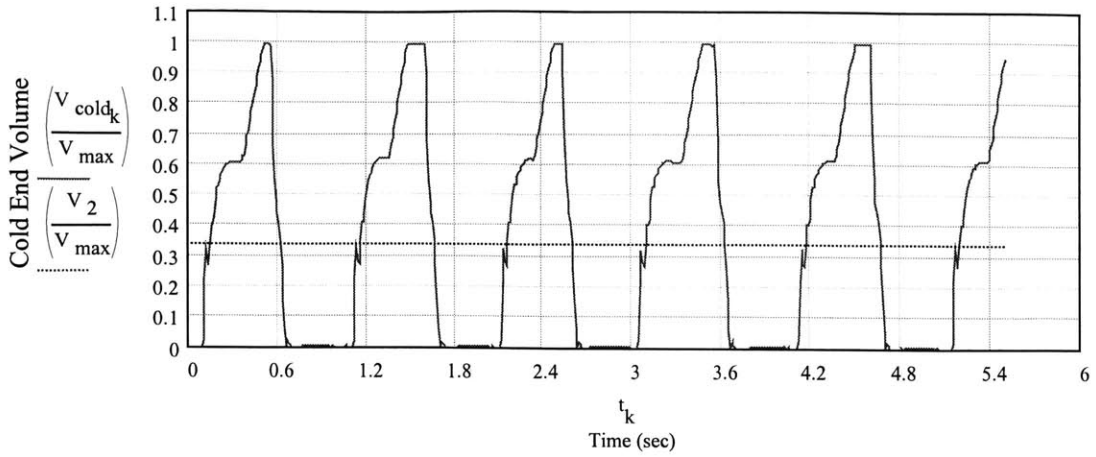

Figure 40: V^*_{cold} vs. Time for Matching Stroke

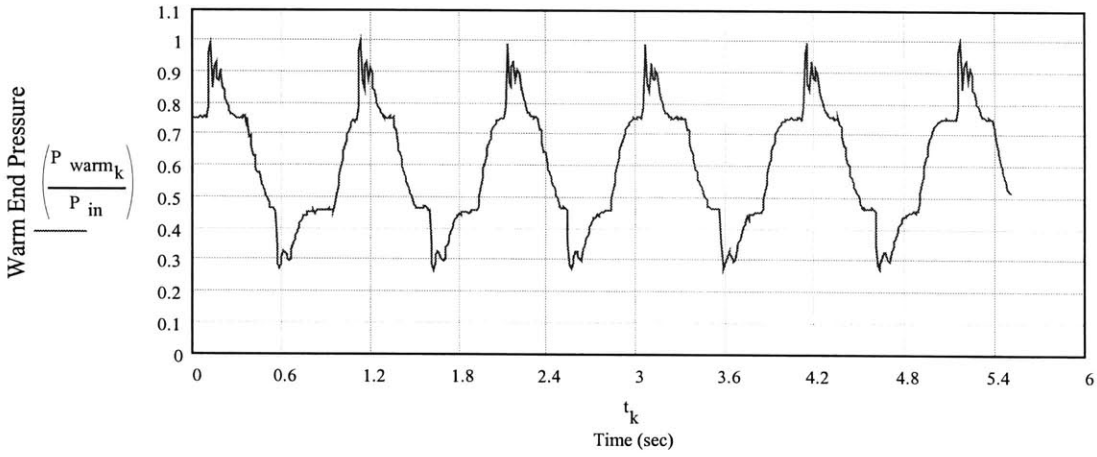

Figure 41: P^*_{warm} vs. Time for Matching Stroke

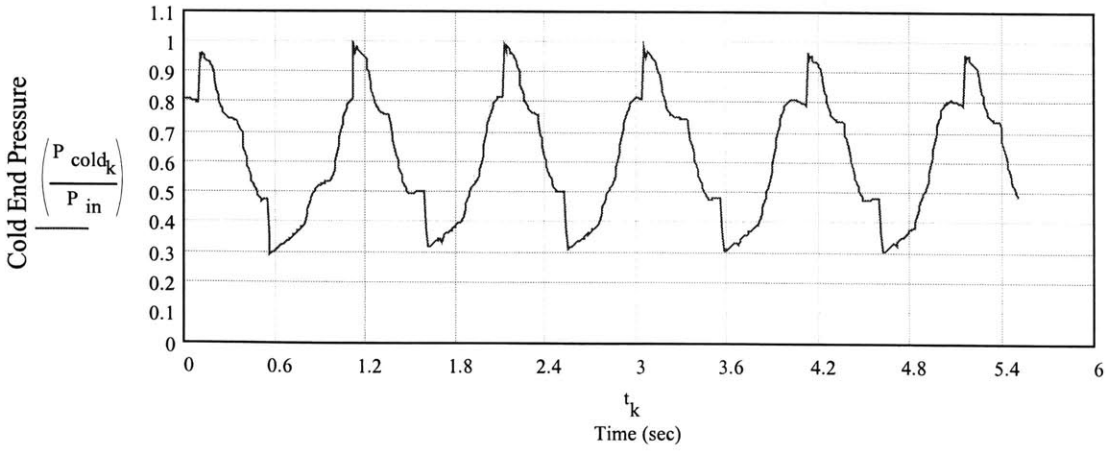

Figure 42: P^*_{cold} vs. Time for Matching Stroke

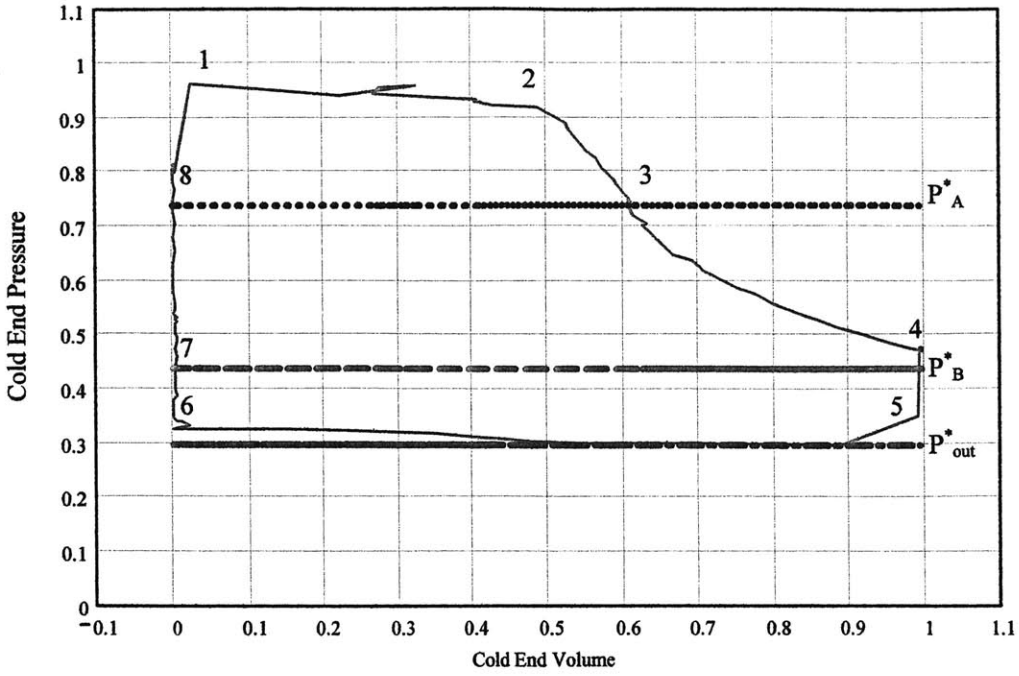

Figure 43: P^*_{cold} vs. V^*_{cold} Plot for Matched Stroke

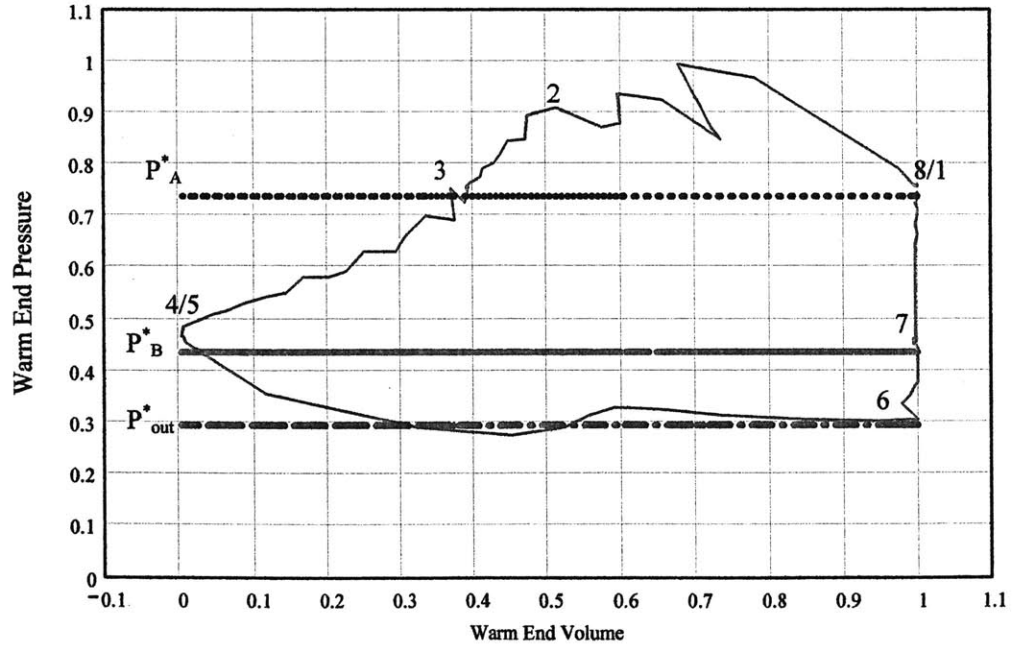

Figure 44: P^*_{warm} vs. V^*_{warm} Plot for Matched Stroke

The P^*_{cold}-V^*_{cold} diagram in Figure 43, looked almost identical to that of Figure 38, except the blow-down process is shifted to occur at V_{max}, V^*_{cold}=1. The results of the work analysis, shown in Table 6, show that again, the P^*_{cold}-V^*_{cold} relationship in the cold region of the expander closely resembled that of the ideal model.

	Ideal Model	Experimental (cold region)
Work Computed (in-lb)	66.5	62.7
Normalized Work (W^*)	1	.94

Table 6: Work Results for Matched Stroke

In Table 6, the work values for the optimized model were not shown because the experimental system parameters did not fit the theoretical criterion for the rubber geometry model.

The final scenario, represented by Figure 45 through Figure 49, showed the system's behavior for a high stroke, when the piston reached top dead center too soon. Although the plots for this scenario looked similar to the matched case scenario, notice the drift in the pressure transducer at state 4 in Figure 48 was not present. This was because the pressure in the cylinder was still changing rapidly when the piston reached top dead center, and there was no drift in the piezo-quartz transducer.

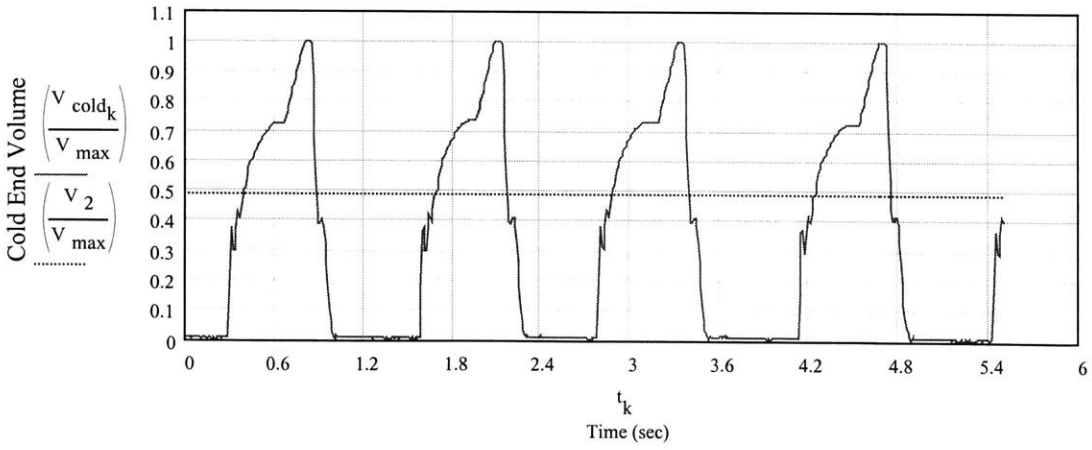

Figure 45: V^*_{cold} vs. Time for High Stroke

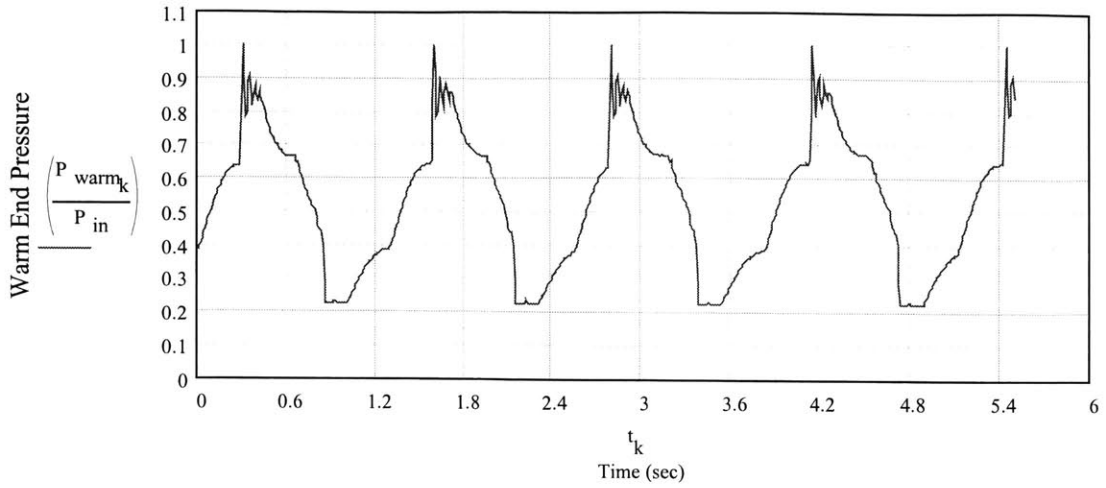

Figure 46: P^*_{warm} vs. Time for High Stroke

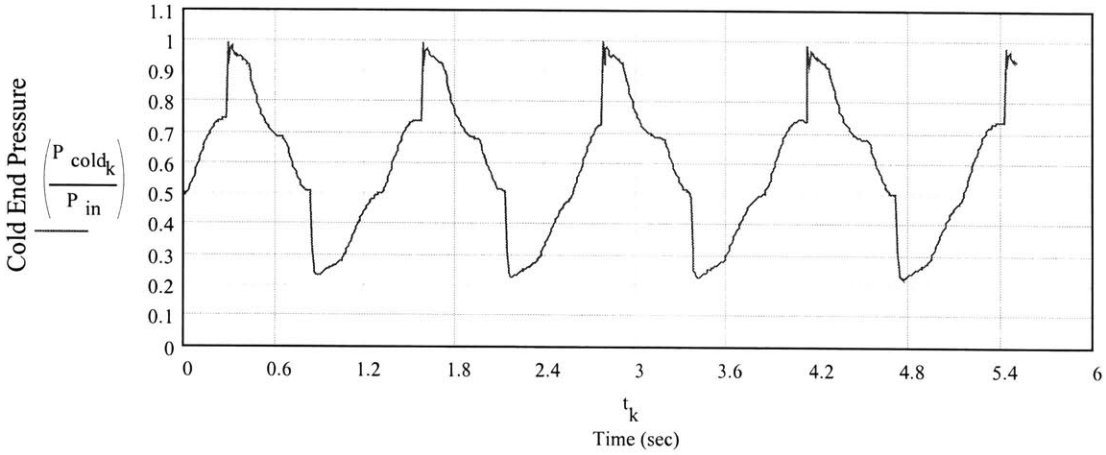

Figure 47: P^*_{cold} vs. Time for High Stroke

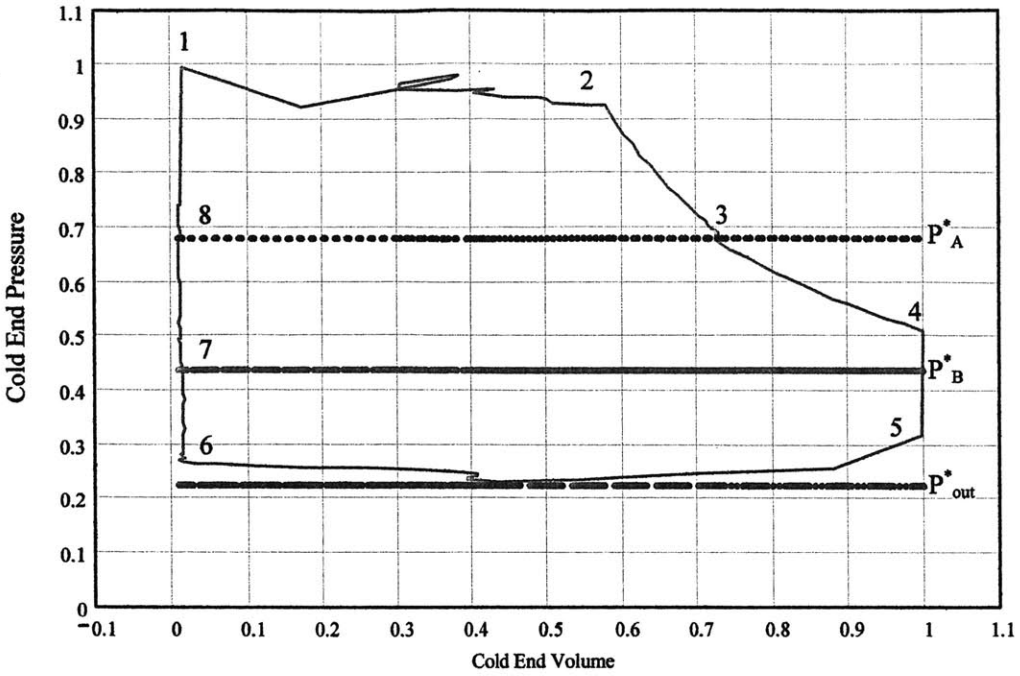

Figure 48: P^*_{cold} vs. V^*_{cold} Plot for High Stroke

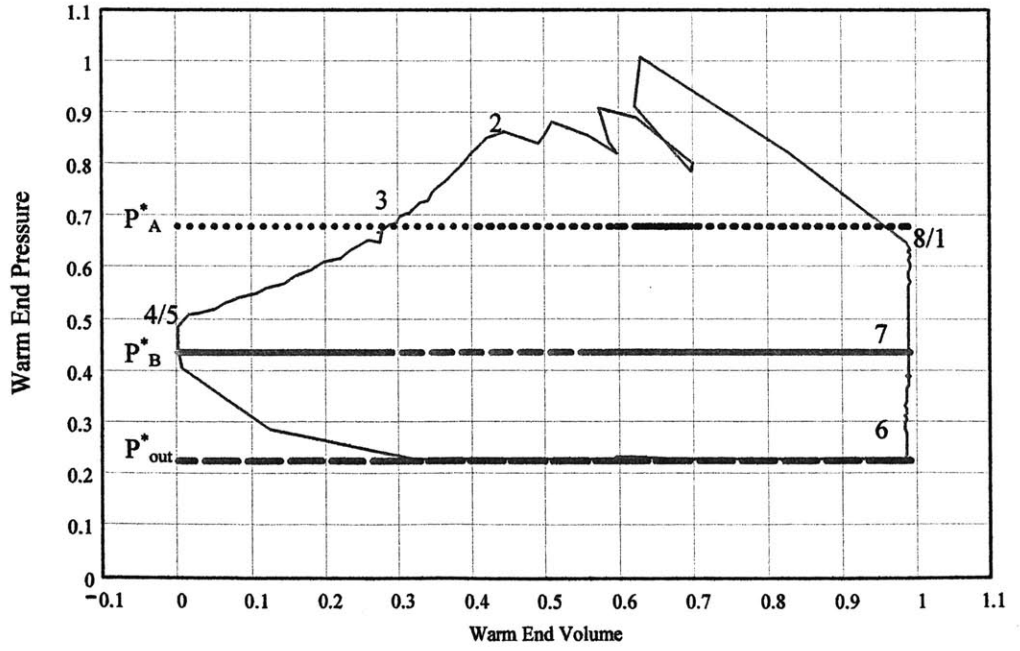

Figure 49: P^*_{warm} vs. V^*_{warm} Plot for High Stroke

	Ideal Model	Optimized Model	Experimental (cold region)
Work Computed (in-lb)	110.5	95.5	99.5
Normalized Work (W^*)	1	.86	.90

Table 7: Work Results for High Stroke

In the Table 7, the optimized model predicted a much closer value to the experimental than was shown in Table 5 because the high stroke model represented the blow-down process better than the low stroke model.

4.3.1 Equilibrium

The next phase of experiments investigated the steady-state cyclic operating conditions of the apparatus. In particular, the equilibrium pressures of the intermediate pressure tanks were determined. To observe these values, the large intermediate pressure tanks were replaced with smaller tanks that manifested the transient behavior of the system over fewer cycles. The new volume ratio, V_{max}/V_{tank}=.047, was sufficient to maintain stability in the system and provided constant pressure reservoirs with only a 5% fluctuation over each cycle.

The unmatched models had predicted several equilibrium combinations of the intermediate pressure tanks for each value of V^*_2. However, when the system was operated with the smaller tanks, the equilibrium pressures were always the same for a given V^*_2.

V^*_2=.5	Initial Pressure	Pressure at 40 cycles	Steady Pressure
Initial Condition 1			
P^*_A	.30	.60	.63
P^*_B	.26	.26	.30
Initial Condition 2			
P^*_A	.92	.73	.63
P^*_B	.26	.38	.30
Initial Condition 3			
P^*_A	.84	.83	.63
P^*_B	.69	.47	.30

Table 8: Transient Response of Intermediate Pressure Tanks

Table 8 illustrated the transient response of the aparatus with the small pressure tanks installed. The tanks were charged with various initial pressures and the system was monitored as the pressures approached cyclic equilibrium. As seen in Table 8, the system returned to the same equilibrium, despite extreme variations on the initial pressures in the tanks. Further tests revealed that the steady-state operating conditions were independent of the cycle speed, which was controlled by variations on the throttling at the warm end of the expander. The testing configurations shown in Figure 12 were also shown to have no effect on the equilibrium conditions. Recall that Figure 12 illustrated two configurations for the 5/2-spool valve. Configuration (I) only used one throttle valve to control the flow to both pressure tanks. Configuration (II) used two throttle valves, one for each tank.

The next stage of experiments was to determine if the steady-state operating conditions corresponded with the matched stroke scenario where the thermal performance was optimized. Figure 50 showed the measured steady-state intermediate pressures for various cyclic speeds.

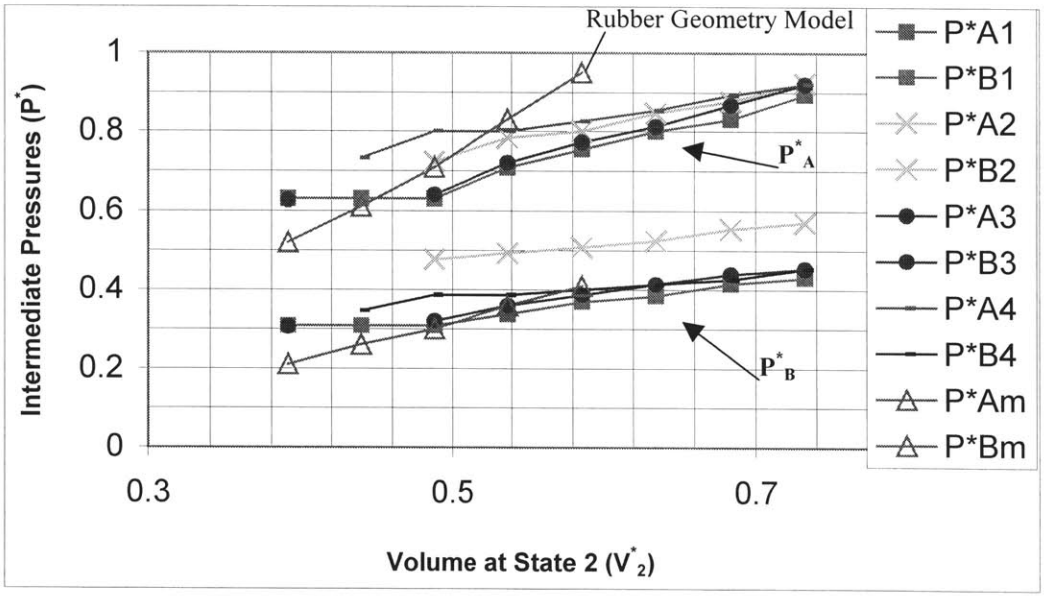

Figure 50: Steady-State Operating Conditions of the Expander (P^*_{out} = .2)

In Figure 50, the upper group of pressures represented the values for P^*_A for various cyclic frequencies. Similarly, the lower group of pressures represented P^*_B. Note that the rubber geometry model did not exceed $V^*_2 \cong (.6)$. This was because P^*_A for the model would have exceeded a value of 1. Consequently, since most of the steady-state pressures for P^*_B were below that of the rubber geometry model, the system operated with a high stroke.

As in the time dependent plots, errors in the control routine can be seen in Figure 50. In particular, the steady-state pressures in Figure 50, labeled P^*_{A1} and P^*_{B1}, were constant for $V^*_2 \leq 0.45$. This was not representative of the actual apparatus. Below certain values of V^*_2, the control routine was unable to sample the data fast enough and close the inlet valve appropriately. Even when $V^*_2 \geq .45$, the preset value did not always correspond with the measured value for V^*_2. For example, in Figure 48, the value for V^*_2 was set to (.48), but the measured value for V^*_2 was approximately (.58). This mismatch in volumes was caused by a combination of the inlet and exhaust valves response time and void space. Notice in Figure 50 that the delay in the response of the exhaust valve would have caused the pressure in tank B to decrease, and consequently, so would the pressure in tank A. An improved valve system and control routine would increase these pressures towards that of the rubber geometry model, which provided the optimum thermal performance of the system.

The convergence of the intermediate pressures revealed that the only independent control variables in the system were P^*_{out} and V^*_2. This meant that for a given P^*_{out}, the system could be optimized as a function of only one programmable variable. Consequently, an optimizing control routine could internally adjust V^*_2 to achieve a minimum T^*_{out}.

4.3.2 Speed

According to the models, the cooling ability of the expander was independent of the cycle speed. However, in reality, the cycle speed of the expander directly effected the cooling power by compensating for the heat leak in the apparatus. Consequently, the next stage of tests determined the limiting factors on the speed of the apparatus.

The lower limit of speed for the expander depended on the viscous leak of the working fluid between the piston and cylinder wall. This viscous leak time constant was determined from the experimental data shown in Figure 51. From the measured values, it was determined that the piston dropped in the static fluid at a rate of .095in/sec. Consequently, to ensure the viscous leak had less than a 10% effect on the position of the piston during one cycle, the expander needed to be operated at a frequency of .6Hz or faster. From Figure 51, it was also determined that the natural frequency of oscillation for the blow-in process was approximately 16Hz as compared to 20Hz which was predicted by the dynamic analysis shown in Figure 34.

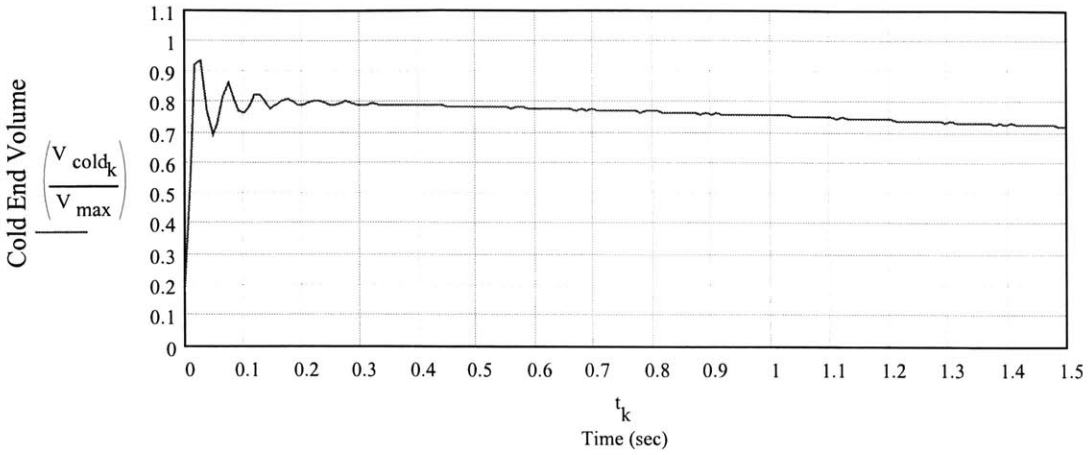

Figure 51: Experimental Dynamics of Blow-in Process

The upper limit of the expander speed was determined experimentally by reducing the throttling effects in the warm region of the expander. The reduced throttling allowed the expansions to occur very rapidly and increased the overall cyclic speed. Figure 52 showed V^*_{cold} as a function of time for the maximum attainable speed of the apparatus.

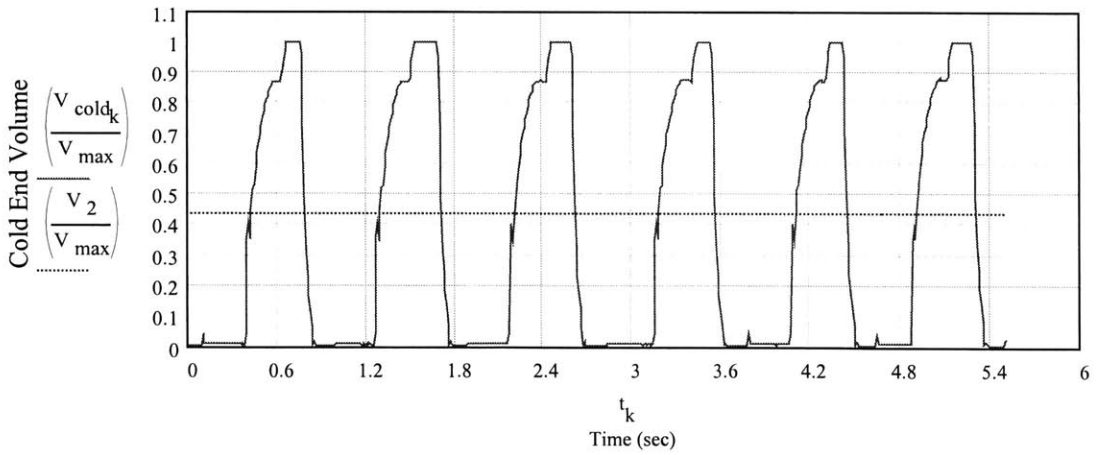

Figure 52: V^*_{cold} vs. Time for Maximum Cycle Speed

The cyclic frequency for the test shown in Figure 52 was approximately 1.3Hz. The major limiting factor on the cycle speed of the experimental apparatus was the control routine. As the speed increased, the data resolution became inadequate to provide consistent control. Although not evident from the tests run with this particular apparatus, the inertia of the piston had a direct effect on the speed of the cycle for a given value of P^*_{out}.

4.3.3 Cooling

As expected, with higher cyclic frequencies, T^*_{out} decreased. Figure 53 showed the inlet and exhaust line temperature plotted as a function of time for the test with the maximum attainable speed. This test produced a T^*_{out} of (.83), which was the lowest of all the experiments.

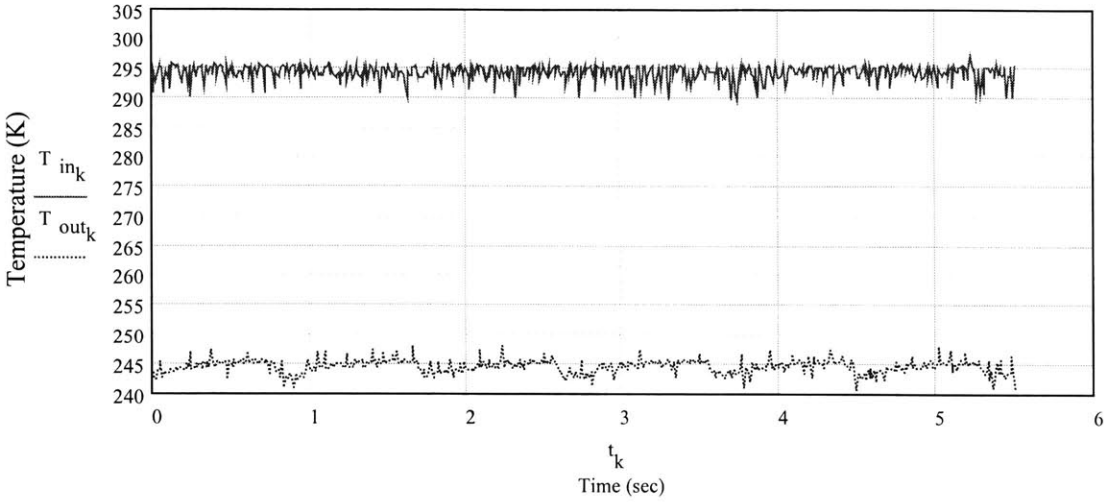

Figure 53: Minimum Experimental Temperature vs. Time (P^*_{out}=.2)

This was a significant temperature drop considering the lack of thermal insulation on the apparatus. The oscillations in the T_{out} plot of Figure 53 represented the blow-down process when the coolest air was blown across the thermocouple. In between cycles, the ambient air filled the exhaust line and caused the temperature to increase slightly.

5 Conclusion

The purpose of this project was to show that a free-piston cryogenic expander could be constructed and controlled reliably. The first stage of the project consisted of thermodynamic and dynamic modeling of the system. The models were then thermally optimized to determine which set of operating parameters would produce the maximum temperature drop in the working fluid. Although the system was not designed for thermal performance, the system's behavior at these optimum operating conditions was critical.

The next stage of the project consisted of fabrication and instrumentation of the system. Being a free-piston apparatus meant sensing and controlling the position of the piston had to be done non-intrusively. A special LVDT was designed and constructed on the cylinder wall to provide real-time feedback to the control routine, which used signals from the LVDT, pressure transducers and thermocouples to control the expander. The control system then used digitally controlled valves on the warm and cold ends of the expander to maintain the desired pressure-volume relation in the cold region of the expander.

Results from the experimental tests were compared with the theoretical thermodynamic and dynamic analysis to determine the expander's performance. Computation of the work represented by the P^*_{cold}-V^*_{cold} diagrams showed that the expander's behavior closely resembled the models and identified design considerations for a second-generation expander. In particular, the experiments showed that the data acquisition and control system needed to be improved in order to obtain adequate data resolution and perform computations throughout the cycle. Despite the limitations, the expander performed well and provided significant cooling under testing conditions.

Appendix A: Normalized Equations

Normalized State Equations

Rubber Geometry:

Warm Region: State 1

$$P_1 = P_{in} \qquad M_1 = M_8$$

$$V_1 = V_{max} \cdot \left(\frac{P_A}{P_{in}}\right)^{\frac{1}{k}} \qquad T_1 = T_8 \cdot \left(\frac{P_{in}}{P_A}\right)^{\frac{k-1}{k}}$$

State 2

$$P_2 = P_{in} \qquad M_2 = M_1 \cdot \frac{V_2}{V_1}$$

$$V_2 = V_{max} - V_{2cold} \qquad T_2 = T_1$$

State 3

$$P_3 = P_A \qquad M_3 = \frac{P_3 \cdot V_3}{T_3}$$

$$V_3 = V_{max} - V_{3cold} \qquad T_3 = T_2 \cdot \left(\frac{P_A}{P_{in}}\right)^{\frac{k-1}{k}}$$

State 4

$$P_4 = P_B \qquad M_4 = 0$$

$$V_4 = 0$$

State 5

$$P_5 = P_{out} \qquad M_5 = 0$$

$$V_5 = 0$$

State 6

$$P_6 = P_{out} \qquad M_6 = \frac{P_{out} \cdot V_{max}}{T_o}$$

$$V_6 = V_{max} \qquad T_6 = T_o$$

State 7

$$P_7 = P_B \qquad M_7 = \frac{P_B \cdot V_{max}}{T_7}$$

$$V_7 = V_{max} \qquad T_7 = \frac{T_6}{\frac{P_6}{P_7} + \frac{1}{k} \cdot \frac{T_6}{T_o} \cdot \left(1 - \frac{P_6}{P_7}\right)}$$

State 8

$$P_8 = P_A \qquad M_8 = \frac{P_A \cdot V_{max}}{T_8}$$

$$V_8 = V_{max} \qquad T_8 = \frac{T_7}{\frac{P_7}{P_7} + \frac{1}{k} \cdot \frac{T_7}{T_o} \cdot \left(1 - \frac{P_7}{P_8}\right)}$$

Cold Region: State 1

$$P_1 = P_{in} \qquad M_1 = \frac{P_{in} \cdot V_1}{T_1}$$

$$V_1 = V_{max} \cdot \left[1 - \left(\frac{P_A}{P_{in}}\right)^{\frac{1}{k}}\right] \qquad T_1 = T_{in} \cdot k \cdot \frac{\left[1 - \left(\frac{P_A}{P_{in}}\right)^{\frac{1}{k}}\right]}{\left[1 - \left(\frac{P_A}{P_{in}}\right)\right]}$$

State 2

$$2 = P_{in} \qquad M_2 = \frac{P_{in} \cdot V_2}{T_2}$$

$$V_2 = \text{Control} \qquad T_2 = \frac{T_{in}}{1 - \frac{V_1}{V_2} \cdot \left(1 - \frac{T_{in}}{T_1}\right)}$$

State 3

$$P_3 = P_A \qquad M_3 = \frac{P_A \cdot V_3}{T_3}$$

$$V_3 = V_2 \cdot \left(\frac{P_i}{P_A}\right)^{\frac{1}{k}} \qquad T_3 = T_2 \cdot \left(\frac{P_A}{P_{in}}\right)^{\frac{k-1}{k}}$$

State 4

$$P_4 = P_B \qquad M_4 = \frac{P_B \cdot V_4}{T_4}$$

$$V_4 = V_{max} \qquad T_4 = T_3 \cdot \left(\frac{P_B}{P_A}\right)^{\frac{k-1}{k}}$$

State 5 Expander

$$P_5 = P_{out} \qquad M_5 = \frac{P_{out} \cdot V_{max}}{T_5}$$

$$V_5 = V_{max} \qquad T_5 = T_4 \cdot \left(\frac{P_{out}}{P_B}\right)^{\frac{k-1}{k}}$$

Exhaust Line

$$P_{5exh} = P_{out} \qquad M_{5exh} = M_4 - M_5$$

$$V_{5exh} = \frac{M_{5exh} \cdot T_{5exh}}{P_{out}} \qquad T_{5exh} = \frac{M_4 \cdot T_4 - M_5 \cdot T_5}{M_{5exh} \cdot k}$$

State 6 Expander

$$P_6 = P_{out} \qquad M_6 = 0$$

$$V_6 = 0$$

Exhaust Line

$$P_{6exh} = P_{out} \qquad M_{6exh} = M_4$$

$$V_{6exh} = \frac{M_{6exh} \cdot T_{6exh}}{P_{out}} \qquad T_{6exh} = \frac{M_5 \cdot T_5 + M_{5exh} \cdot T_{5exh}}{M_4}$$

State 7

$$P_7 = P_B \qquad M_7 = 0$$

$$V_7 = 0$$

State 8

$$P_8 = P_A \qquad M_8 = 0 \qquad V_8 = 0$$

Fixed Geometry: (changed states different from rubber geometry)

V_2 set HIGH

Cold Region: State 4

$$P_4 = P_3 \cdot \left(\frac{V_3}{V_{max}}\right)^k \qquad M_4 = \frac{P_4 \cdot V_{max}}{T_4}$$

$$V_4 = V_{max} \qquad T_4 = T_3 \cdot \left(\frac{V_3}{V_{max}}\right)^{k-1}$$

V_2 set LOW

Warm Region: State 4

$$P_4 = P_B \qquad M_4 = \frac{P_B \cdot V_4}{T_4}$$

$$V_4 = V_{max} - V_{4cold} \qquad T_4 = T_3 \cdot \left(\frac{P_B}{P_3}\right)^{\frac{k-1}{k}}$$

State 5

$$P_5 = P_{out} \qquad M_5 = \frac{P_{out} \cdot V_5}{T_5}$$

$$V_5 = V_4 \cdot \left(\frac{P_4}{P_{out}}\right)^{\frac{1}{k}} \qquad T_5 = T_4 \cdot \left(\frac{P_{out}}{P_4}\right)^{\frac{k-1}{k}}$$

State 6

$$P_6 = P_{out} \quad M_6 = \frac{P_{out} \cdot V_{max}}{T_6} \qquad V_6 = V_{max}$$

$$T_6 = \frac{T_o \cdot k \cdot V_{max}}{V_{max} + (k-1) \cdot V_5 - \frac{M_5}{P_{out}} \cdot (T_5 - T_o \cdot k)}$$

Cold Region: State 4

$$P_4 = P_B \qquad M_4 = \frac{P_B \cdot V_4}{T_4}$$

$$V_4 = V_3 \cdot \left(\frac{P_3}{P_B}\right)^{\frac{1}{k}} \qquad T_4 = T_3 \cdot \left(\frac{P_B}{P_3}\right)^{\frac{k-1}{k}}$$

State 5 Expander

$$P_5 = P_{out} \qquad M_5 = \frac{P_{out} \cdot V_{max}}{T_5}$$

$$V_5 = V_{max} - V_{5warm} \qquad T_5 = T_4 \cdot \left(\frac{P_{out}}{P_4}\right)^{\frac{k-1}{k}}$$

Exhaust Line

$$P_{5exh} = P_{out} \quad M_{5exh} = M_4 - M_5 \quad V_{5exh} = \frac{M_{5exh} T_{5exh}}{P_{out}}$$

$$T_{5exh} = \frac{M_4 \cdot T_4 - M_5 \cdot T_5 + M_{4warm}\left(T_{4warm} - T_{5warm}\right)}{M_{5exh} \cdot k}$$

Appendix B: Single Equation Opitmization

Single equation for final temperature of free-piston expander

Rubber Geometry Model

$V_{max} := 1 \qquad P_{in} := 1 \qquad T_{in} := 1 \qquad P_{out} := .1 \qquad k := 1.666$

$$T_{6exh}(V_2, P_A, P_B) := \frac{\frac{V_2 \cdot T_{in}}{k \cdot V_{max}} \cdot \left(\frac{P_{out}}{P_{in}}\right) \cdot \left(\frac{P_B}{P_{in}}\right)^{\frac{-2}{k}} \cdot \left[(k-1) + \frac{P_B}{P_{out}}\right]}{1 - \frac{V_{max}}{V_2 \cdot k} \cdot \left[k \cdot \left[1 - \left(\frac{P_A}{P_{in}}\right)^{\frac{1}{k}}\right] - \left(1 - \frac{P_A}{P_{in}}\right)\right]}$$

for matched case, V2(Pb, Pout), and Pa and Pb are related throught the mass balance, therefore T(Pa or Pb)

$P_{B_0} := .1 \qquad j := 0..450$

Guess for Pa:

$P_A := .9 \qquad P_{B_{j+1}} := P_{B_j} + .001$

$$Pa_j := root\left[\left[\left(k - 1 + \frac{P_A}{P_{B_j}}\right) \cdot \left[1 - \left(\frac{P_A}{P_{B_j}}\right)^{\frac{-1}{k}}\right] - 1 + -(k-1) \cdot \frac{P_{out}}{P_{B_j}}\right], P_A\right]$$

Yields Pa(Pb), based on mass balance

$$T_{6exh}(P_A, P_B) := \frac{\frac{P_B^{\frac{1}{k}} \cdot T_{in}}{k} \cdot (P_{out}) \cdot (P_B)^{\frac{-2}{k}} \cdot \left[(k-1) + \frac{P_B}{P_{out}}\right]}{1 - \frac{1}{P_B^{\frac{1}{k}} \cdot k} \cdot \left[k \cdot \left[1 - (P_A)^{\frac{1}{k}}\right] - (1 - P_A)\right]}$$

Determines final exhaust line temperature of fluid as a function of matched pressures.

$$V_{2_j} := \left(P_{B_j}\right)^{\frac{1}{k}}$$

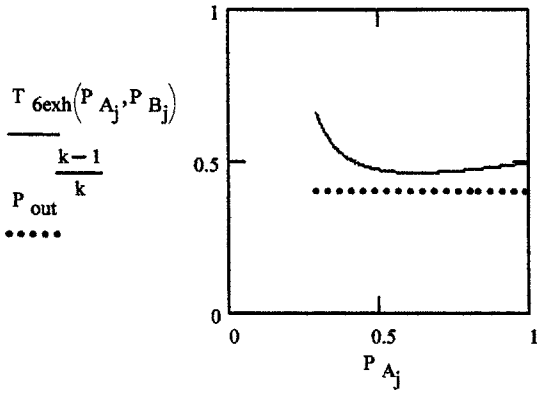

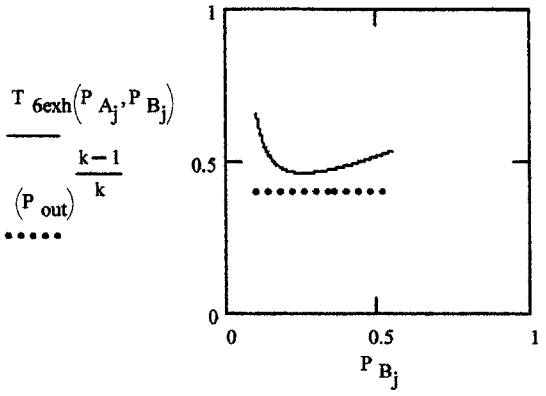

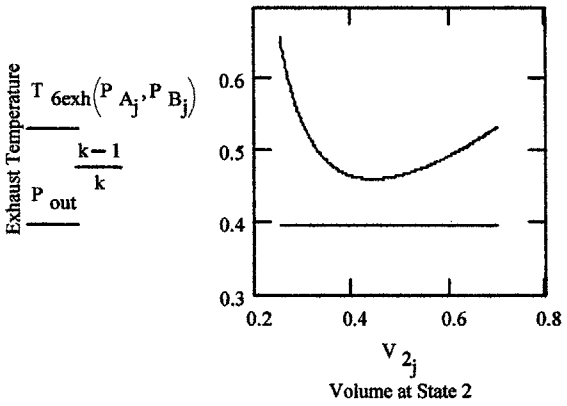

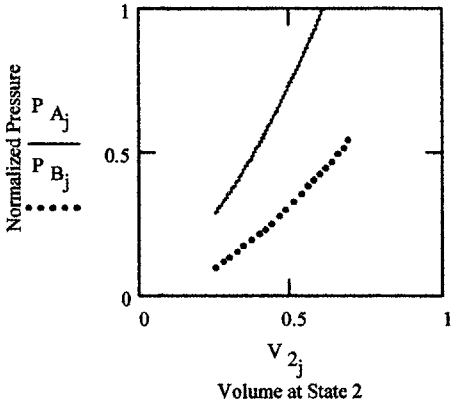

$$Sol_j := T_{6exh}\left(P_{A_j}, P_{B_j}\right)$$

$$\min(Sol) = 0.46151$$

adjust to match

$$ww := 157$$

$$Sol_{ww} = 0.462$$

$$V_2 := \left(P_{B_{ww}}\right)^{\frac{1}{k}} \qquad T_{out} := Sol_{ww}$$

$$P_B := P_{B_{ww}} \qquad P_A := P_{A_{ww}}$$

Check mass balance

$$\left[\left(k-1+\frac{P_A}{P_B}\right)\cdot\left[1-\left(\frac{P_B}{P_A}\right)^{\frac{1}{k}}\right]-1+-(k-1)\cdot\frac{P_{out}}{P_B}\right]=1.77375\cdot10^{-6}$$

RESULTS:

$P_{in}=1$ $\quad V_2=0.442$

$P_A=0.619$ $\quad T_{out}=0.462$

$P_B=0.257$

$P_{out}=0.1$

Appendix C: Calibration Curves for Instruments

$$T(emf) := 1.702252510 \cdot emf - .2209724 emf^2 \ldots + .0054809314 emf^3 - .000057669892 emf^4 + 273$$

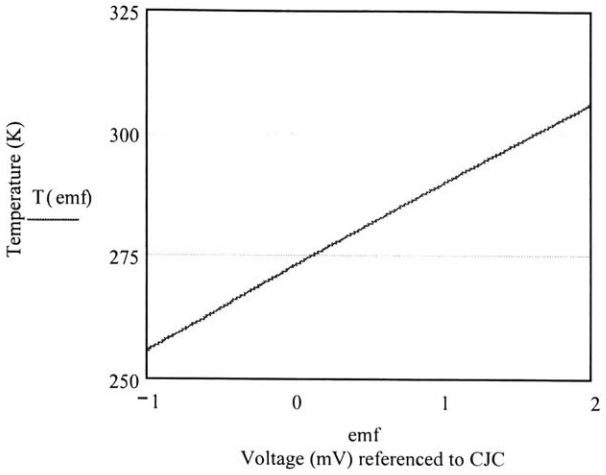

Figure 54: Calibration for Type "E" Thermocouple

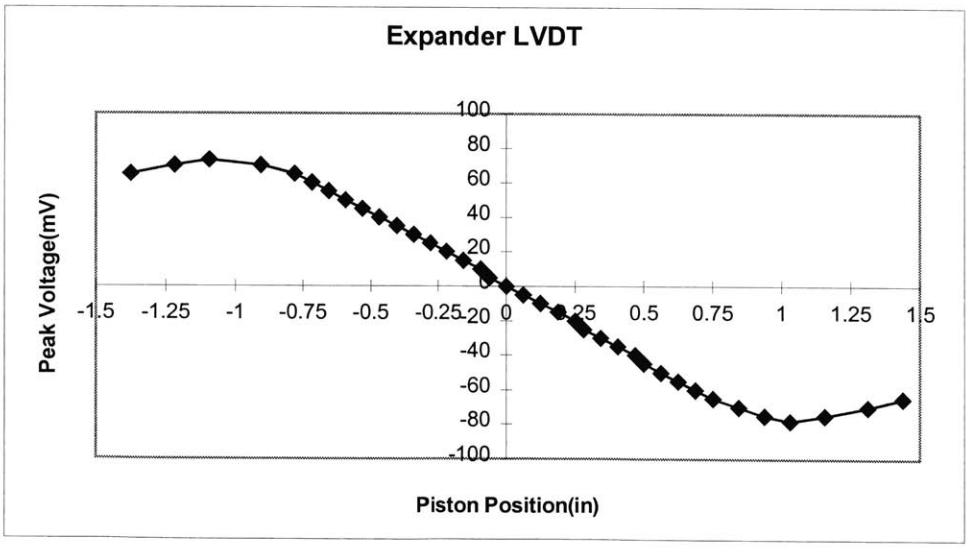

Figure 55: Calibration for Linear Variable Differential Transformer

Appendix D: QBasic control program

```
''''''''''''''''''''''''''''''''''''''''''''''''''''''''''''''''
'    Ryan Edward Jones     Master's in Mechanical Enginnering
'    RJCNTRL.BAS - Manual/Automatic Control program for
'              free piston expander project
'    Modified: 7/14/98
'    MetraByte Corporation   DAS20 - Data Acquisition Card
'    Started writing 6/22/98
''''''''''''''''''''''''''''''''''''''''''''''''''''''''''''''''


        DIM DIO%(10), TEMP%(100), P(10000)
        DIM DT%(100), CH%(100)  'set up integer arrays for data/channel

        COMMON SHARED DIO%(), DT%(), CH%(), TEMP%()
        DECLARE SUB DAS20 (MODE%, BYVAL dummy%, FLAG%)

        '$DYNAMIC
        DIM dat%(10000)
        '$STATIC


'---------- Initialize section -------------------------------------

        SCREEN 0, 0, 0: CLS : KEY OFF: WIDTH 80


200 '----- Initialize with mode 0 ---------------------------------

220 OPEN "C:\DAS\DAS20.ADR" FOR INPUT AS #1  'get base I/O address
230 INPUT #1, DIO%(0)
240 DIO%(1) = 7                'interrupt level
250 DIO%(2) = 1                'D.M.A. level
270 FLAG% = 0                  'error variable
280 MD% = 0                    'mode 0 - initialize
290 CALL DAS20(MD%, VARPTR(DIO%(0)), FLAG%)
300 IF FLAG% <> 0 THEN PRINT "INSTALLATION ERROR # "; FLAG%: STOP

320 '----- Write manual operation instructions to the screen --------

325 CLS
330 LOCATE 1, 1: PRINT "Operation Mode: MANUAL"
340 LOCATE 3, 22: PRINT "Status:"
350 LOCATE 5, 5: PRINT "I - Inlet valve  Closed"
360 LOCATE 6, 5: PRINT "E - Exit valve   Closed"
370 LOCATE 7, 5: PRINT "T - Tank toggle  Tank A"
380 LOCATE 10, 5: PRINT "A - Write data to A:\"
390 LOCATE 9, 5: PRINT "B - Begin automatic operation"
```

```
400 LOCATE 13, 5: PRINT "X - Terminate program"

405 '---- digital output initialization ----------------------------
410 DIO%(0) = 7
415 GOTO 800

420 '----- Determine key press for manual operation ----------------

430 M$ = INKEY$: IF M$ = "" GOTO 430

440 IF M$ = "I" OR M$ = "i" THEN GOTO 450 ELSE GOTO 500
450 LOCATE 5, 22: IF (DIO%(0) AND 1) = 0 THEN GOTO 480
460 DIO%(0) = DIO%(0) - 1: PRINT "Open  "
470 GOTO 800
480 DIO%(0) = DIO%(0) + 1: PRINT "Closed": GOTO 800

500 IF M$ = "E" OR M$ = "e" THEN GOTO 510 ELSE GOTO 550
510 LOCATE 6, 22: IF (DIO%(0) AND 2) = 0 THEN GOTO 540
520 DIO%(0) = DIO%(0) - 2: PRINT "Open  "
530 GOTO 800
540 DIO%(0) = DIO%(0) + 2: PRINT "Closed": GOTO 800

550 IF M$ = "T" OR M$ = "t" THEN GOTO 560 ELSE GOTO 600
560 LOCATE 7, 22: IF (DIO%(0) AND 4) = 0 THEN GOTO 590
570 DIO%(0) = DIO%(0) - 4: PRINT "Tank B"
580 GOTO 800
590 DIO%(0) = DIO%(0) + 4: PRINT "Tank A": GOTO 800

600 IF M$ = "A" OR M$ = "a" THEN LOCATE 17, 1 ELSE GOTO 730
610 PRINT "Transfering data to file": OPEN "A:\OUTPUT.DAT" FOR OUTPUT AS #2
611 WRITE #2, X2
612 WRITE #2, DTPT
620 FOR K = 0 TO DTPT
630 WRITE #2, P(K)
640 NEXT K
645 CLOSE #2
650 LOCATE 17, 1: PRINT "Data transfer complete  "
660 GOTO 420

730 IF M$ = "B" OR M$ = "b" THEN DOUT = DIO%(0): GOTO 1000

740 IF M$ = "X" OR M$ = "x" THEN STOP
750 GOTO 420

790 '----- Digital output routine ---------------------------------

800 MD% = 15
810 CALL DAS20(MD%, VARPTR(DIO%(0)), FLAG%)
820 IF FLAG% <> 0 THEN PRINT "Error # "; FLAG%; " on digital output"
830 GOTO 420

1000  '---- Setting A/D pacer clock --------------------------------

1010 DIO%(0) = 2000      ' This divides 5MHz by the two input values
1020 DIO%(1) = 0
1030 MD% = 24
```

```
1040 CALL DAS20(MD%, VARPTR(DIO%(0)), FLAG%)
1050 IF FLAG% <> 0 THEN PRINT "Error #"; FLAG%; " in setting timer": STOP

1060 '---- Load ADC control queue-----------------------------------

1070 MD% = 1
1080 DIO%(0) = 0              'Set channel
1090 DIO%(1) = 4              'Select gain
1100 DIO%(2) = 2              'Set as first entry in queue
1110 CALL DAS20(MD%, VARPTR(DIO%(0)), FLAG%)
1115 IF FLAG% <> 0 THEN PRINT "Error #"; FLAG%; " in setting queue": STOP
1120 DIO%(0) = 2              'Select channel
1130 DIO%(1) = 0              'Select gain
1140 DIO%(2) = 0              'Set as normal entry in queue
1150 CALL DAS20(MD%, VARPTR(DIO%(0)), FLAG%)
1155 IF FLAG% <> 0 THEN PRINT "Error #"; FLAG%; " in setting queue": STOP
1160 DIO%(0) = 3              'Select channel
1170 DIO%(1) = 3              'Select gain
1180 DIO%(2) = 0              'Set as normal entry in queue
1190 CALL DAS20(MD%, VARPTR(DIO%(0)), FLAG%)
1195 IF FLAG% <> 0 THEN PRINT "Error #"; FLAG%; " in setting queue": STOP
1200 DIO%(0) = 5              'Select channel
1210 DIO%(1) = 7              'Select gain
1220 DIO%(2) = 0              'Set as normal entry in queue
1230 CALL DAS20(MD%, VARPTR(DIO%(0)), FLAG%)
1235 IF FLAG% <> 0 THEN PRINT "Error #"; FLAG%; " in setting queue": STOP
1240 DIO%(0) = 6              'Select channel
1250 DIO%(1) = 7              'Select gain
1260 DIO%(2) = 0              'Set as normal entry in queue
1270 CALL DAS20(MD%, VARPTR(DIO%(0)), FLAG%)
1275 IF FLAG% <> 0 THEN PRINT "Error #"; FLAG%; " in setting queue": STOP
1280 DIO%(0) = 7              'Select channel
1290 DIO%(1) = 0              'Select gain
1300 DIO%(2) = 1              'Set as last entry in queue
1310 CALL DAS20(MD%, VARPTR(DIO%(0)), FLAG%)
1315 IF FLAG% <> 0 THEN PRINT "Error #"; FLAG%; " in setting queue": STOP

1320 '---- Write automatic operation instructions to the screen------

1330 CLS
1340 LOCATE 1, 1: PRINT "Operation Mode: AUTOMATIC"
1350 LOCATE 3, 5: PRINT "U - Increase X2"
1360 LOCATE 4, 5: PRINT "D - Decrease X2"
1370 LOCATE 6, 5: PRINT "W - Write data to memory"
1380 LOCATE 8, 5: PRINT "S - Stop automatic operation/Return to Manual"

1390 '---- Initialize variables for automatic operation -------------

1400 X2 = 2500: STPT = 1: DTPT = 3599: INC = 100
1410 DPR = 1: DV = 1: DX = 40: CW = 3: XMIN = 0: TDV = 0
1420 WTL = 1600: SC = 0: AC = 0: XX = 0

1600 '---- Obtain ADC values and store in DT%( ) ---------------------

1605 LOCATE 4, 50: PRINT "X2 = "; X2
1610 MD% = 4
```

```
1620 DIO%(0) = 6                'Number of Conversions
1630 DIO%(1) = VARPTR(DT%(0))   'Provide array location write to
1640 DIO%(2) = 2                'Internal timer/No gate
1650 CALL DAS20(MD%, VARPTR(DIO%(0)), FLAG%)
1660 IF FLAG% <> 0 THEN PRINT "Error #"; FLAG%; " in mode 4": STOP

1670 '---- Stop internal timer for ADC ------------------------------

1680 MD% = 26
1690 DIO%(0) = 0                'Stop A/D timer
1700 CALL DAS20(MD%, VARPTR(DIO%(0)), FLAG%)

1710 '---- Signal monitoring and controls loop ----------------------

1790 LOCATE 10, 1
1800 FOR KK = 0 TO 5
1810 PRINT DT%(KK), TEMP%(KK)
1820 NEXT KK

2000 IF X <> 0 THEN GOTO 12000

3000 IF ABS(DT%(0) - TEMP%(0)) > DV THEN GOTO 9000

4000 IF ABS(DT%(1) - TEMP%(1)) > DPR THEN GOTO 13000

5000 IF ABS(DT%(0) - XMIN) > DX THEN GOTO 7000

6000 IF DOUT = 1 THEN DOUT = 3: GOTO 8000
6010 IF DOUT = 3 THEN DOUT = 7: GOTO 8000
6020 IF DOUT = 7 THEN DOUT = 6: GOTO 8000
6030 GOTO 11000

7000 IF DOUT = 7 THEN DOUT = 3: GOTO 8000
7010 IF DOUT = 3 THEN DOUT = 1: GOTO 8000
7020 GOTO 11000

8000 MD% = 15
8010 DIO%(0) = DOUT
8020 CALL DAS20(MD%, VARPTR(DIO%(0)), FLAG%)
8030 IF FLAG% <> 0 THEN PRINT "Error # "; FLAG%; " on digital output"
8040 X = CW: GOTO 13000

9000 IF DOUT <> 6 THEN GOTO 13000

10000 IF (DT%(0) - X2) < 0 THEN GOTO 13000
10010 DOUT = 7: GOTO 8000

11000 LOCATE 20, 1: PRINT "ILLEGAL SIGNAL!!!!": SLEEP: GOTO 320

12000 X = X - 1

13000 FOR K = 0 TO 5: TEMP%(K) = DT%(K)
13010 NEXT K
13020 FOR TD = 0 TO TDV
13030 NEXT TD
```

```
20000 '--- Determine key press for automatic operation ----------

20010 A$ = INKEY$: LOCATE 4, 50
20020 IF A$ = "U" OR A$ = "u" THEN X2 = (X2 + INC): PRINT "X2 = "; X2
20030 IF A$ = "D" OR A$ = "d" THEN X2 = (X2 - INC): PRINT "X2 = "; X2
20040 IF A$ = "S" OR A$ = "s" THEN GOTO 320
20049 LOCATE 19, 1
20050 IF A$ = "W" OR A$ = "w" THEN WTL = 20100: PRINT TIME$
20060 IF WTL = 1600 THEN GOTO 1600
20070 IF WTL = 20100 THEN GOTO 20100

20100 '--- Check for counter to save data ---------------------------

20110 SC = SC + 1
20120 IF SC = STPT THEN GOTO 30000 ELSE GOTO 1600

30000 '--- Saving data to array P() subroutine ----------------------

30010 FOR K = AC TO (AC + 5)
30015 P(K) = TEMP%(K - AC)
30020 NEXT K
30030 AC = AC + 6: SC = 0
30040 IF AC > DTPT THEN GOTO 30200
30050 LOCATE 17, 1: PRINT "Saving data": GOTO 1600

30200 WTL = 1600: AC = 0
30210 LOCATE 20, 1: PRINT TIME$
30220 LOCATE 17, 1: PRINT "           ": GOTO 1600

50000 END
```

Appendix E: Data Manipulation Worksheet

Data Manipulation Worksheet

Data Descriptin: Data file:

Gage Pressure:

$P_{out} := 14.7$

$P_{in} := 35 + P_{out}$ $P_A := 22 + P_{out}$ $P_B := 7 + P_{out}$ $elapse := 5.5$

Read Data from Disk and store in arrays

$j := 0 .. 50000$

$data_j := READ("Output15.dat")$

$X2R := data_0$ $DTPT := data_1$ $kp := \frac{DTPT + 1}{6} - 1$

$k := 0 .. (kp)$

$X_k := data_{(k \cdot 6)+2}$ $P1_k := data_{(k \cdot 6+1)+2}$ $T2_k := data_{(k \cdot 6+3)+2}$ $t_k := \frac{k}{kp} \cdot elapse$

$CJC_k := data_{(k \cdot 6+5)+2}$ $P2_k := data_{(k \cdot 6+2)+2}$ $T1_k := data_{(k \cdot 6+4)+2}$

$$FF(DD, CC) := \left| \begin{array}{l} \text{for } w \in 0 .. CC \\ \quad \left| \begin{array}{l} DD_w \leftarrow DD_w \text{ if } DD_w < 2048 \\ DD_w \leftarrow -(4096 - DD_w) \text{ if } DD_w > 2048 \end{array} \right. \\ DD \end{array} \right.$$

$T1 := FF(T1, kp)$ $T2 := FF(T2, kp)$ $P2 := FF(P2, kp)$

Calibration Curves:

Position:

$XP(XD) := 1.528 \cdot \frac{XD}{4096}$ $X2 := XP(X2R)$

$Vol(XD) := \frac{1.5^2}{4} \cdot \pi \cdot XD \cdot \frac{1.528}{4096}$ $Vmax := Vol(4096)$

Temperature: Type "E" Thermocouples referenced to CJC

T[K] emf[mV]

$$T(emf) := 1.702252510 \cdot emf - .2209724 emf^2 ... + .0054809314 emf^3 - .000057669892 emf^4 + 273$$

Pressure: $PW(PD) := \frac{PD}{2048} \cdot 200 + PWA$ $SL := \frac{P_{in} - 14.7}{\max(P2) - \min(P2)}$ $LL := \min(P2)$

$PC(P2) := (SL \cdot P2 - LL \cdot SL) + 14.7 + PCA$

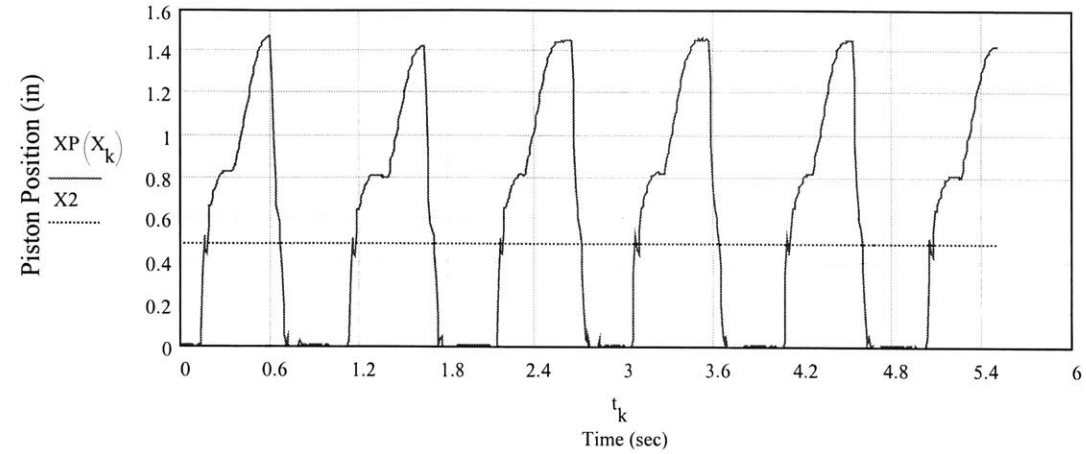

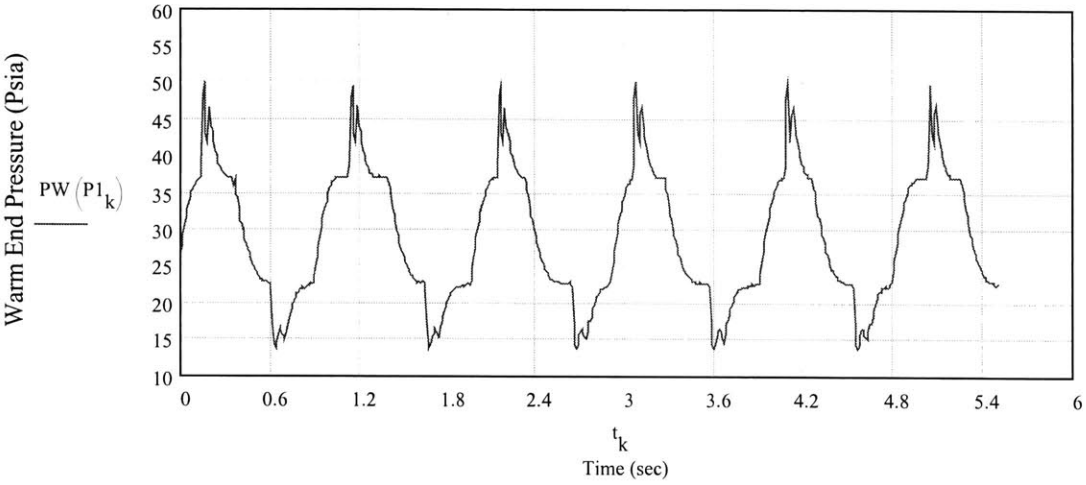

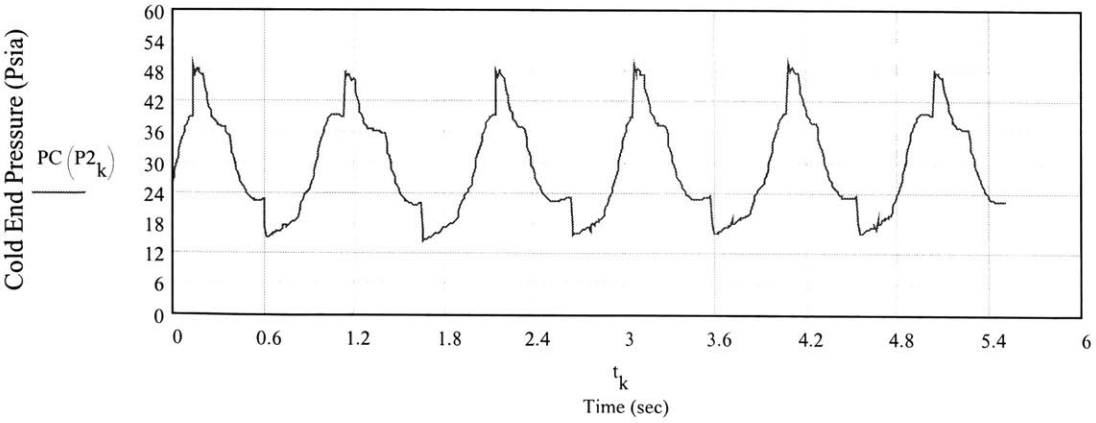

$$emf1_k := T1_k \cdot \frac{50}{2048} \qquad emf2_k := T2_k \cdot \frac{50}{2048}$$

$$Tin_k := T\left(emf1_k\right) \qquad Tout_k := T\left(emf2_k\right)$$

$$T_{in} := \left[\frac{\sum_{j=0}^{kp} Tin_j}{kp+1} \right] \qquad T_{out} := \left[\frac{\sum_{j=0}^{kp} Tout_j}{kp+1} \right]$$

$$\frac{T_{out}}{T_{in}} = 0.901$$

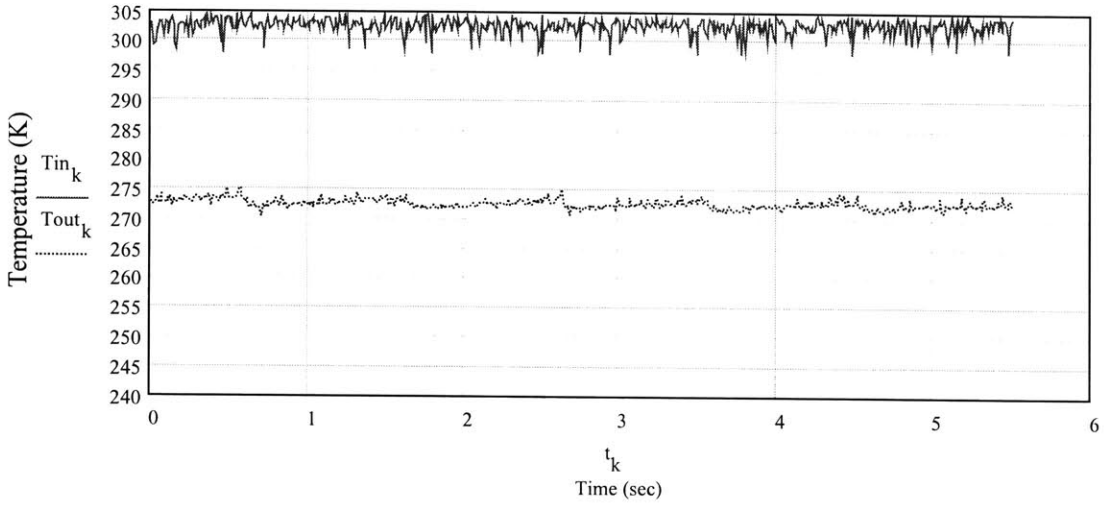

kf := 99

k := 0.. kf t_{kf} = 0.909 $(t_{kf})^{-1}$ = 1.1 Vol(X2R) = 0.857

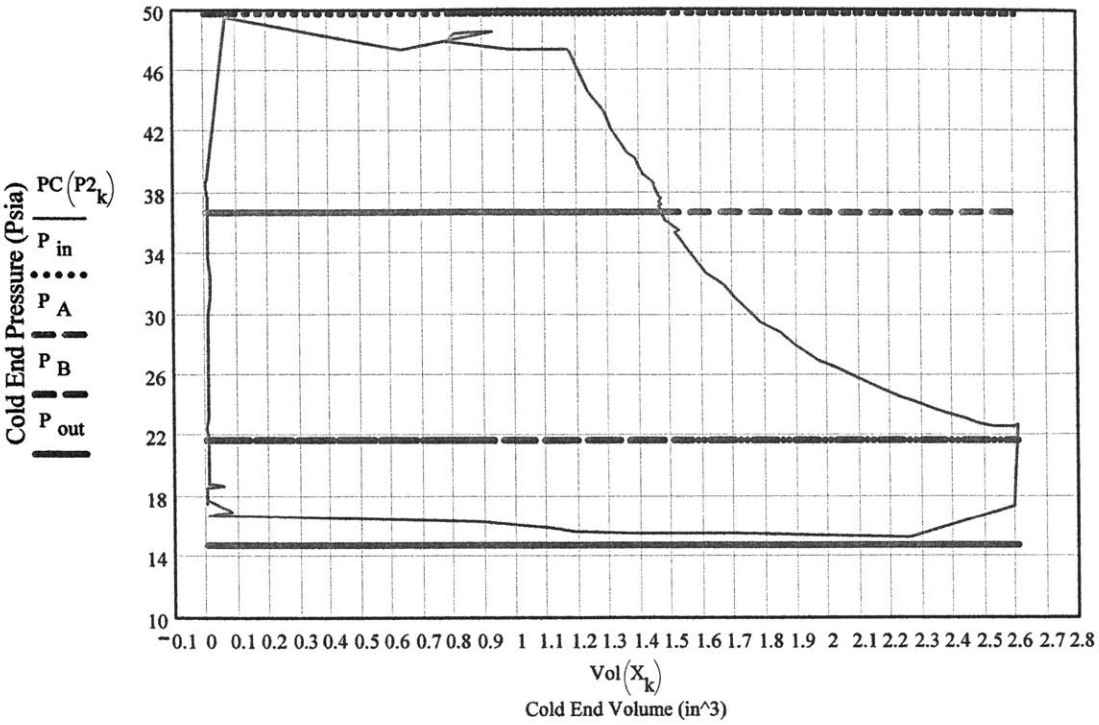

k := 0.. kf t_{kf} = 0.909 $(t_{kf})^{-1}$ = 1.1 Adjust: PCA≡0 PWA≡0

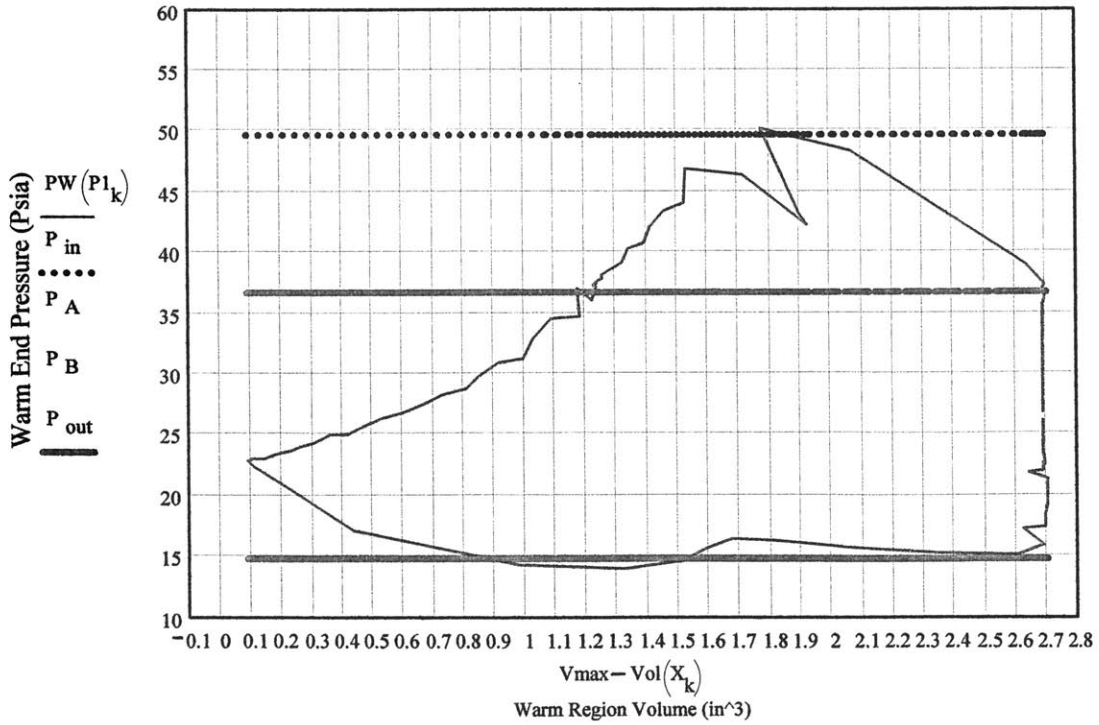

Calculating the work transfer from the ideal/warm/cold:

SET:

$$Work := \begin{bmatrix} 0 \\ 0 \end{bmatrix} \qquad V2 := Vol(X2R) \qquad V2 = 0.857 \qquad V2 := 1.25 \qquad V_{final} := Vmax$$

$$IntPdV(Work) := \left| \begin{array}{l} \text{for } jj \in 0..kf \\ \quad AW \leftarrow \dfrac{\left(PW\left(P1_{jj+1}\right) + PW\left(P1_{jj}\right)\right)\cdot\left(Vol\left(X_{jj+1}\right) - Vol\left(X_{jj}\right)\right)}{2} \\ \quad Work_0 \leftarrow Work_0 + AW \\ \quad AC \leftarrow \dfrac{\left(PC\left(P2_{jj+1}\right) + PC\left(P2_{jj}\right)\right)\cdot\left(Vol\left(X_{jj+1}\right) - Vol\left(X_{jj}\right)\right)}{2} \\ \quad Work_1 \leftarrow Work_1 + AC \\ Work \end{array} \right.$$

$$IntPdV(Work) = \begin{bmatrix} 55.137 \\ 57.431 \end{bmatrix} \qquad W_{warm} := IntPdV(Work)_0 \qquad W_{cold} := IntPdV(Work)_1$$

$$W_{ideal} := P_{in}\cdot V2 - P_{out}\cdot Vmax + \frac{P_{in}\cdot V2}{1.7-1}\left[1 - \left(\frac{V2}{Vmax}\right)^{1.7-1}\right]$$

WORK COMPARISONS:

$W_{ideal} = 59.418$

$W_{cold} = 57.431$

$W_{warm} = 55.137$

$$\frac{W_{warm}}{W_{cold}} = 0.96$$

$$\frac{W_{cold}}{W_{ideal}} = 0.967$$

$$\frac{W_{warm}}{W_{ideal}} = 0.928$$

Appendix F: Dynamic Analysis Worksheet

Solution to 8-1 process:

Fluid Properties

$Cp := 5192.6\frac{joule}{kg \cdot K}$ $\rho := 1\cdot\frac{kg}{m^3}$

$Cv := 3115.6\frac{joule}{kg \cdot K}$

$\mu := 1.95\cdot 10^{-5}\cdot\left(\frac{kg}{m^2}\cdot\frac{m}{sec^2}\right)\cdot sec$

$k := \frac{Cp}{Cv}$

Piston/Cylinder Dimensions

$D := 1.49\cdot in$ $mp := .5\cdot kg$ $G := .008\cdot m$

$L := .5\cdot m$

$h := .1\cdot m$

$Pi := 4\cdot 10^5\cdot\frac{kg}{m^2}\cdot\frac{m}{sec^2}$ $A_s := \pi\cdot D\cdot L$

$g := 9.8\cdot\frac{m}{sec^2}$ $A_c := \pi\cdot\left(\frac{D}{2}\right)^2$

$P8 := 3\cdot 10^5\cdot\frac{kg}{m^2}\cdot\frac{m}{sec^2}$ $A_o := \frac{A_c}{100}$

$\beta := \frac{\rho\cdot A_c^{\,3}\cdot\frac{m}{sec}}{2\cdot A_o^{\,2}\cdot mp\cdot 2}$ $\omega 0 := \sqrt{\frac{k\cdot A_c\cdot P8}{mp\cdot h}}$ $F := \frac{Pi\cdot A_c}{mp} - g$

$C := F$

Forcing time constant:

$\tau := .05\cdot sec$

$\beta = 5.625\cdot sec^{-1}$

$\omega 0 = 106.063\cdot sec^{-1}$

$\omega 1 := \sqrt{\omega 0^2 - \beta^2}$ $\omega 1 = 105.913\cdot sec^{-1}$

$$x(t) := \frac{C}{\beta^2 + \omega 1^2} + \frac{-C\cdot e^{-\frac{t}{\tau}}}{\left(-\frac{1}{\tau} + \beta\right)^2 + \omega 1^2} + \frac{C\cdot e^{-\beta\cdot t}}{\tau\cdot\omega 1}\cdot\frac{\left(\beta^2 - \omega 1^2 - \frac{\beta}{\tau}\right)\cdot\sin(\omega 1\cdot t) + \omega 1\cdot\left(2\cdot\beta - \frac{1}{\tau}\right)\cdot\cos(\omega 1\cdot t)}{\left(\beta^2 - \omega 1^2 - \frac{\beta}{\tau}\right)^2 + \left[\omega 1\cdot\left(2\cdot\beta - \frac{1}{\tau}\right)\right]^2}$$

$t := 0\cdot sec, .001\cdot sec .. 1\cdot sec$

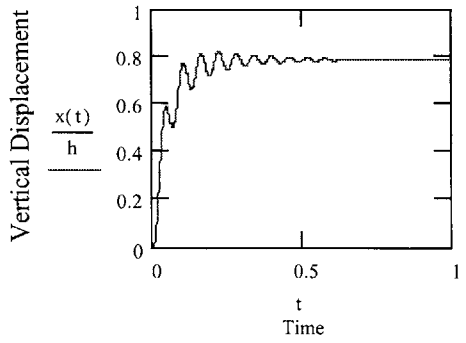

Linear approx. of Bernouli's Eqt. for the orifice

References

1. **Bejan, Adrian**, *Advanced Engineering Thermodynamics*, John Wiley & Sons, New York, 1988
2. **Boles, Micheal A.**, and □**engel, Yunus A.**, *Thermodynamics, an Engineering Approach*, McGraw-Hill, New York, 1994
3. **Collins, S.C.**, and **Cannaday, R.L.**, *Expansion Machines for Low Temperature Processes*, Oxford University Press, New York, 1958
4. **Hildebrand, Francis B.**, *Advanced Calculus for Applications*, Prentice-Hall, Inc., New Jersey, 1976
5. **Incropera, Frank P.**, and **DeWitt, David P.**, *Fundamentals of Heat and Mass Transfer*, John Wiley & Sons, New York, 1990
6. **Johnson, David E., Johnson, Johnny R.**, **Hilburn, John L.**, and **Scott, Peter D.**, *Electric Circuit Analysis*, Prentice-Hall, Inc., New Jersey, 1997
7. **Ludwigsen, Jill L.**, *Configuration and Testing of a Saturated Vapor Helium Compressor*, M.S., 1985, Smith/Iwasa
8. **Marion, Jerry B.**, *Classical Dynamics of Particles and Systems*, Academic Press, Inc., New York, 1970
9. **Mills, A.F.**, *Heat and Mass Transfer*, Irwin, Chicago, 1995
10. Minuteman Controls Catalog # 197, Massachusetts, 1997, p. 540
11. **Scott, R.B.**, *Cryogenic Engineering*, Met-Chem Research, Inc., Colorado, 1988
12. **Urieli, I., and Berchowitz, D.M.**, *Stirling Cycle Engine Analysis*, Adam Hilger Ltd., Bristol, 1984